

NRROS negatively regulates reactive oxygen species during host defence and autoimmunity

Rajkumar Noubade^{1†}, Kit Wong¹, Naruhisa Ota¹, Sascha Rutz¹, Celine Eidenschenk¹, Patricia A. Valdez^{1†}, Jiabing Ding¹, Ivan Peng¹, Andrew Sebrell², Patrick Caplazi³, Jason DeVoss¹, Robert H. Soriano⁴, Tao Sai², Rongze Lu¹, Zora Modrusan⁴, Jason Hackney⁵ & Wenjun Ouyang¹

Reactive oxygen species (ROS) produced by phagocytes are essential for host defence against bacterial and fungal infections. Individuals with defective ROS production machinery develop chronic granulomatous disease^{1,2}. Conversely, excessive ROS can cause collateral tissue damage during inflammatory processes and therefore needs to be tightly regulated. Here we describe a protein, we termed negative regulator of ROS (NRROS), which limits ROS generation by phagocytes during inflammatory responses. NRROS expression in phagocytes can be repressed by inflammatory signals. NRROS-deficient phagocytes produce increased ROS upon inflammatory challenges, and mice lacking NRROS in their phagocytes show enhanced bactericidal activity against *Escherichia coli* and *Listeria monocytogenes*. Conversely, these mice develop severe experimental autoimmune encephalomyelitis owing to oxidative tissue damage in the central nervous system. Mechanistically, NRROS is localized to the endoplasmic reticulum, where it directly interacts with nascent NOX2 (also known as gp91^{phox} and encoded by *Cybb*) monomer, one of the membrane-bound subunits of the NADPH oxidase complex, and facilitates the degradation of NOX2 through the endoplasmic-reticulum-associated degradation pathway. Thus, NRROS provides a hitherto undefined mechanism for regulating ROS production—one that enables phagocytes to produce higher amounts of ROS, if required to control invading pathogens, while minimizing unwanted collateral tissue damage.

In response to microorganisms and inflammatory stimuli, professional phagocytes can generate ROS either within mitochondria or through a process named oxidative burst mediated by the NADPH oxidase 2 (NOX2) complex^{1–3}. Although many regulatory factors for ROS production in phagocytes have been described, our knowledge about its precise control is still limited^{1,4–6}. Although priming bone marrow-derived macrophages (BMDMs) with either interferon-γ (IFN-γ) or lipopolysaccharide (LPS) was sufficient to induce ROS upon subsequent zymosan stimulation, treatment with a combination of IFN-γ and LPS had a synergistic effect (Fig. 1a)^{7–9}. Although IFN-γ or LPS could enhance the expression of NOX2 (ref. 9), we speculated that there might be other mechanisms controlling this synergistic ROS production in phagocytes. Gene expression analysis by microarray under these conditions identified a previously uncharacterized gene, EMSMUSG 00000052384, which we named *Nrros* (negative regulator of ROS, previously known as *Lrrc33*) that was markedly downregulated upon priming with a combination of IFN-γ and LPS (Extended Data Fig. 1a). The predicted structure of NRROS contains a signal sequence, 21 putative leucine-rich repeat domains, a transmembrane domain, and a short cytoplasmic domain. NRROS was preferentially expressed in immune organs such as lymph nodes, thymus and spleen in mice (Extended Data Fig. 1b, c). Among leukocytes, myeloid cell subsets including macrophages, neutrophils and dendritic cells had the highest NRROS expression

(Fig. 1b and Extended Data Fig. 1d, e). Interestingly, priming with a combination of IFN-γ and LPS or tumour necrosis factor (TNF)-α alone markedly repressed *Nrros* messenger RNA and protein expression in wild-type BMDMs (Fig. 1c, d).

To reveal the biological functions of NRROS, we generated NRROS-specific antibody and NRROS-deficient mice (Extended Data Fig. 1f–j). At 6 weeks of age, all mice were viable and immune organs and leukocyte subsets were indistinguishable from those of wild-type mice (Extended Data Table 1 and data not shown). However, significantly augmented ROS production was observed from NRROS-deficient primary BMDMs upon zymosan stimulation after priming for 24 h with either IFN-γ (Fig. 1e) or LPS (Fig. 1f). These observations were confirmed in a variety of phagocytes, under several priming and activation

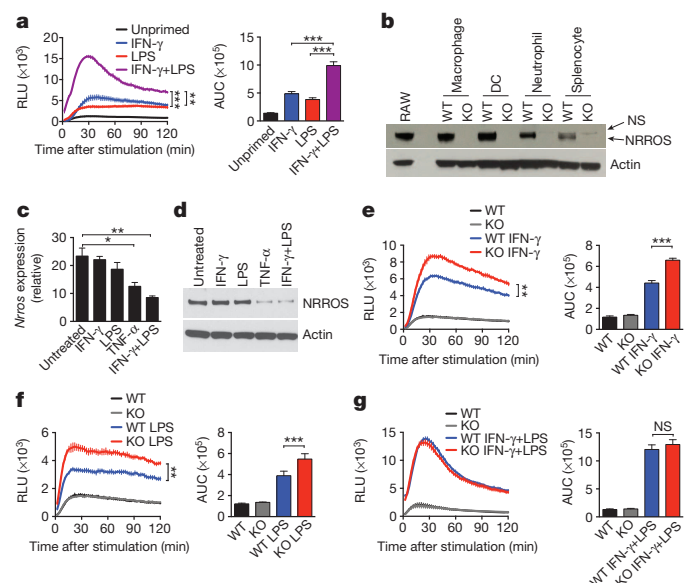


Figure 1 | NRROS is a negative regulator of ROS in phagocytes.

a, Zymosan-induced ROS production in BMDMs primed as indicated. **b**, NRROS expression analysis by western blot in immune cells. Actin was used as loading control. KO, NRROS-deficient knockout; NS, nonspecific band; WT, wild type. **c, d**, mRNA (**c**) and protein (**d**) of NRROS in BMDMs treated as indicated. **e–g**, Zymosan-induced ROS production in WT and KO BMDMs primed with IFN-γ (**e**), LPS (**f**) or both (**g**). **a, e–g**, Left, ROS kinetic plots of a representative experiment with three independent samples per group. Right, averaged area under curve (AUC) from five independent experiments. Error bars, s.e.m. *P < 0.05, **P < 0.01, ***P < 0.001. Unpaired Student's t-test with Welch's corrections, (**a, e–g**, left), paired Student's t-test (**a, e–g**, right), unpaired Student's t-test (**c**). RLU, relative light units. Data in **b–d** represent at least three independent experiments.

¹Department of Immunology, Genentech Inc., 1 DNA Way, South San Francisco, California 94080, USA. ²Department of Antibody Engineering, Genentech Inc., 1 DNA Way, South San Francisco, California 94080, USA. ³Department of Pathology, Genentech Inc., 1 DNA Way, South San Francisco, California 94080, USA. ⁴Department of Molecular Biology, Genentech Inc., 1 DNA Way, South San Francisco, California 94080, USA. ⁵Department of Bioinformatics, Genentech Inc., 1 DNA Way, South San Francisco, California 94080, USA (R.N.). [†]Present addresses: Flexus Biosciences, 75 Shoreway Road, Suite D, San Carlos, California 94070, USA (R.N.); American Society for Biochemistry and Molecular Biology, 11200 Rockville Pike, Suite 302, Rockville, Maryland 20852, USA (P.A.V.).

conditions using multiple ROS detection methods (Extended Data Fig. 2). Interestingly, priming with a combination of IFN- γ and LPS, a condition that markedly repressed NRROS expression, attenuated the ROS-production difference between wild-type and NRROS-deficient cells (Fig. 1g), supporting the concept that inflammatory signals could control ROS production by regulating NRROS expression. Finally, NRROS exhibited a similar expression pattern and regulation in human cells (Extended Data Fig. 3a–c), and short interfering RNA (siRNA)-mediated knockdown of NRROS in human monocyte-derived macrophages also resulted in increased ROS production (Extended Data Fig. 3d–h). Taken together, these results suggested that NRROS functioned as a general negative regulator of ROS production in phagocytes.

Increased ROS production from NRROS-deficient BMDMs was also observed upon challenge with bacterial pathogens, including *E. coli*, *Salmonella enterica* serovar Typhimurium (hereafter *S. typhimurium*) and heat-killed *L. monocytogenes* (Fig. 2a–c and Extended Data Fig. 4a–c). More importantly, NRROS-deficient BMDMs and neutrophils were highly bactericidal *in vitro* (Fig. 2d and Extended Data Fig. 4d), which was not due to increased nitric oxide production or defective phagocytosis (Extended Data Fig. 4e, f). Conversely, enhanced bacterial killing by NRROS-deficient macrophages was eliminated upon pre-treatment

with diphenyleneiodonium, an inhibitor of ROS production (Fig. 2e). ROS is known to contribute to controlling *L. monocytogenes* infection, especially at higher bacterial burden^{10,11}. At a dose at which most wild-type mice succumbed, most NRROS-deficient mice survived the infection (Fig. 2f). Further, NRROS expression in splenic myeloid cells during infection, even though detectable, was highly repressed (Extended Data Fig. 4g). In accordance with our *in vitro* data, ROS production was significantly higher in spleens of infected NRROS-deficient mice (Fig. 2g). Importantly, survival of NRROS-deficient mice correlated with significantly reduced *L. monocytogenes* burden in livers and spleens of these mice (Fig. 2h). Similar enhanced bacterial killing was also observed upon inoculation of NRROS-deficient mice with live *E. coli* (data not shown). The protective effects observed in NRROS-deficient mice during *L. monocytogenes* infection were completely abrogated when the mice were crossed to NOX2-deficient mice or treated with ROS scavengers (Fig. 2i–k)¹², suggesting that increased ROS production in NRROS-deficient phagocytes contributed to the enhanced host defence against invading pathogens.

Despite the beneficial role in host defence, increased ROS production can also cause collateral tissue damage. As a negative regulator, NRROS might be required to control excessive ROS production during inflammation. Indeed, NRROS-deficient bone marrow chimaeric mice showed enhanced disease severity and high mortality in a myelin oligodendrocyte glycoprotein (MOG)_{35–55}-complete Freund's adjuvant (CFA)-induced experimental autoimmune encephalomyelitis (EAE) model (Fig. 3a, b). A similar high severity of EAE was observed in phagocyte-specific NRROS-deficient mice (*Nrrros*^{f/f} LysM-Cre^{pos}) (Extended Data Fig. 5a–c), excluding a possible contribution of T cells, especially T_H17 cells, in this phenotype^{13,14}. Histological analysis revealed markedly increased lesion severity in *Nrrros*^{f/f} LysM-Cre^{pos} mice compared to control mice (Extended Data Fig. 5d, e). Central nervous system (CNS)-infiltrating leukocytes—especially CD11b⁺ myeloid subsets—from NRROS-deficient bone marrow chimaeric mice showed significantly increased ROS production (Fig. 3c, d). Levels of malondialdehyde, one of the major toxic products of lipid peroxidation and indicator of oxidative damage¹⁵, were significantly higher in the CNS tissues from NRROS-deficient mice than in those from wild-type mice (Fig. 3e, f). Finally, treatment with ROS scavengers after EAE induction reduced disease severity and abrogated the difference between wild-type and NRROS-deficient bone marrow chimaeric mice (Fig. 3g) or *Nrrros*^{f/f} LysM-Cre^{pos} mice (Extended Data Fig. 5f, g), supporting the premise that the increased disease severity in NRROS-deficient mice was caused by augmented tissue oxidation and damage. In summary, these data demonstrated an indispensable role for phagocyte-specific NRROS in limiting ROS-induced tissue damage under inflammatory conditions.

Next we investigated how NRROS regulates ROS production from myeloid cells. We did not detect any differences in mitochondrial ROS (mROS) generation despite an increased total ROS production in NRROS-deficient BMDMs treated with IFN- γ and zymosan (Fig. 4a) or with mROS-specific stimulators, such as antimycin A and rotenone (Extended Data Fig. 6a, b). Conversely, pharmacological inhibition of NOX2 but not of mROS production largely abrogated the differential ROS generation between wild-type and NRROS-deficient BMDMs (Extended Data Fig. 6c–g), implying that NRROS specifically regulates the function of the NOX2 complex. The NOX2 complex is composed of two membrane-bound subunits, NOX2 and p22^{phox} (encoded by *Cyba*) and four cytosolic subunits, p40^{phox}, p47^{phox}, p67^{phox} and RAC (RAC1 or RAC2)^{1,2,8,16}. NOX2 and p22^{phox} form a heterodimer known as flavocytochrome *b*₅₅₈ in the endoplasmic reticulum (ER), and this heterodimerization is essential for the stability of these proteins^{17,18}. In NRROS-deficient BMDMs, the expression, phosphorylation and activation of the cytoplasmic subunits were comparable to those of wild-type BMDMs (Extended Data Fig. 7a–c). However, protein, but not mRNA, levels of NOX2 and p22^{phox} were increased in NRROS-deficient BMDMs (Fig. 4b and Extended Data Fig. 7d, e). Similarly, an increased expression of NOX2 and p22^{phox} was observed in various primary

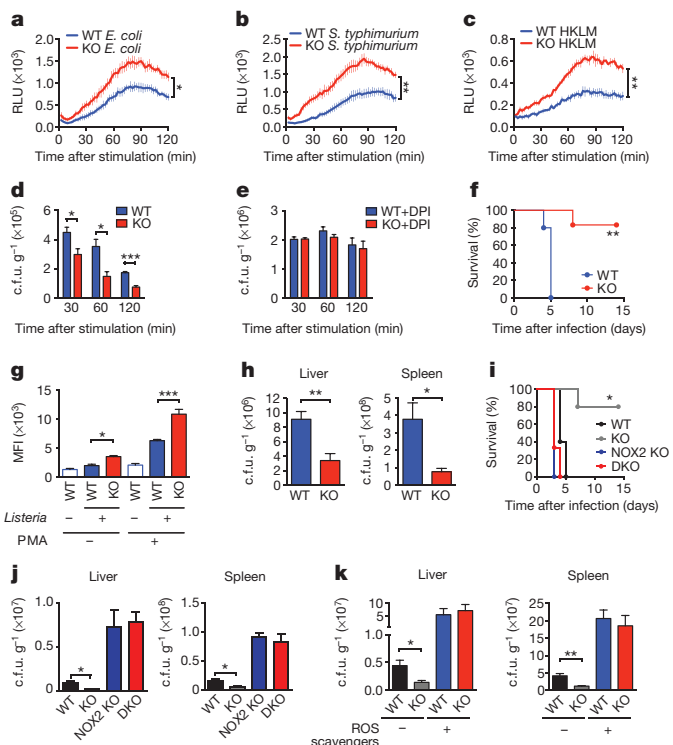


Figure 2 | Increased ROS and bactericidal ability in NRROS-deficient phagocytes. **a–c**, ROS production in WT and NRROS-deficient (KO) BMDMs stimulated *in vitro* with *E. coli* (a), *S. typhimurium* (b) or heat-killed *Listeria monocytogenes* (HKLM; c). **d, e**, *In vitro* *E. coli* killing by IFN- γ -primed WT and KO BMDMs without (d) or with (e) diphenyleneiodonium (DPI) pre-treatment. **f**, Survival curve of *L. monocytogenes*-infected WT ($n = 5$) and KO ($n = 6$) mice. **g**, Ex vivo ROS production by *L. monocytogenes*-infected WT and KO splenocytes ($n = 3$). **h**, *L. monocytogenes* burden in liver and spleen of WT ($n = 5$) and KO ($n = 6$) mice. **i**, Survival curve of *L. monocytogenes*-infected WT ($n = 5$), KO ($n = 6$), NOX2-deficient (NOX2 KO) ($n = 5$) and NRROS NOX2 double-deficient (DKO) ($n = 3$) mice. **j**, *L. monocytogenes* burden in liver and spleen of WT, KO, NOX2 and DKO mice ($n = 3$). **k**, *L. monocytogenes* burden in liver and spleen of WT and KO mice ($n = 5$) pre-treated with ROS scavenger cocktail. Error bars, s.e.m. * $P < 0.05$, ** $P < 0.01$, *** $P < 0.001$. Unpaired Student's *t*-test with (a–c) and without (d, e, g, h, j, k) Welch's corrections, log-rank (Mantel-Cox) test (f, i). c.f.u., colony-forming units. Data are representative of three (a–f, h) and two (g, i–k) independent experiments.

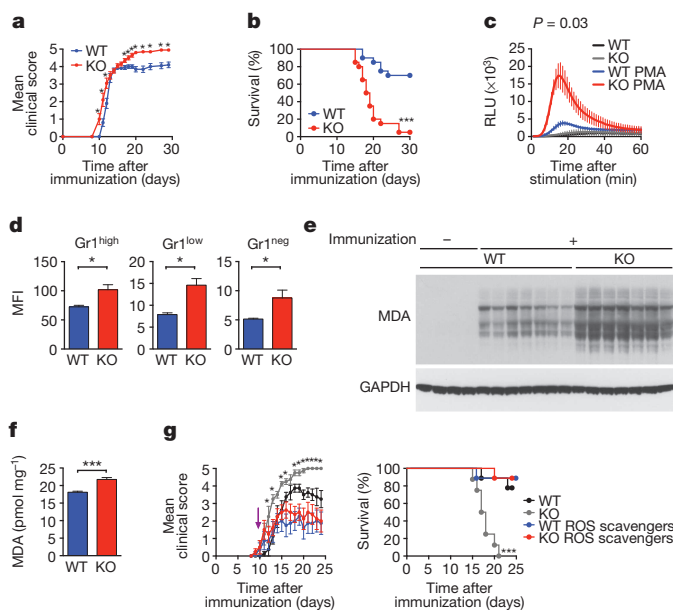


Figure 3 | Mice with NRROS-deficient haematopoietic cells develop severe EAE owing to oxidative damage in the CNS. **a, b,** Clinical course (**a**) and survival curve (**b**) of WT and NRROS-deficient (KO) bone marrow chimaera mice immunized with MOG_{35–55}-CFA ($n = 20$). **c,** ROS production in CNS cells from EAE-induced mice ($n = 4$ WT, 3 KO). **d,** ROS production in CD11b⁺ CNS cells from EAE-induced mice analysed by fluorescence-activated cell sorting ($n = 5$). MFI, mean fluorescence intensity. **e, f,** Malondialdehyde (MDA) adducts in the CNS tissues of EAE-induced mice analysed by western blot (**e**) and enzyme-linked immunosorbent assay (ELISA) (**f**) ($n = 7$). GAPDH as loading control. **g,** Clinical course (left) and survival curve (right) of EAE-induced mice ($n = 9$) treated with a ROS scavenger cocktail from day 10 (arrow). Error bars, s.e.m. * $P < 0.05$, ** $P < 0.01$, *** $P < 0.001$. Unpaired Student's *t*-test without (**a, d, f, g**) and with (**c**) Welch's corrections, log-rank (Mantel-Cox) test (**b, g**). Data are representative of two (**c-g**) and four (**a, b**) independent experiments.

phagocytes from NRROS-deficient mice after inflammatory challenges *in vivo* (Extended Data Fig. 7f-h), supporting a role for NRROS in regulating protein expression or stability of the flavocytochrome b_{558} subunits in phagocytes.

To better understand how NRROS regulates the expression of NOX2 and p22^{phox} proteins, BMDMs were treated with cycloheximide to block *de novo* protein synthesis. NOX2 and p22^{phox} were markedly stabilized for extended durations in NRROS-deficient BMDMs compared to wild-type cells upon treatment (Fig. 4c), suggesting that NRROS participated in the degradation of these proteins. If not dimerized, NOX2 and p22^{phox} are presumed to be quickly degraded through a proteasome-dependent ER-associated degradation (ERAD) pathway^{17–19}. However, upon translocation out of the ER to phagosomal and plasma membranes, the NOX2-p22^{phox} complex might also get degraded by other mechanisms, such as the lysosome-associated degradation pathway. Interestingly, the proteasome inhibitor MG132, but not the lysosome blocker chloroquine, normalized the differences in NOX2 or p22^{phox} protein expression between wild-type and NRROS-deficient BMDMs (Fig. 4d, e and Extended Data Fig. 8a-e). Subcellular fractionation revealed that the accumulation of NOX2 and p22^{phox} in NRROS-deficient cells started in the ER (Fig. 4f). In addition, most NOX2 detected in BMDMs was the 58-kDa ER-bound form (Fig. 4f)²⁰, which was sensitive to both Peptide-N-glycosidase F (PNGase F) and Endoglycosidase H (Endo H) enzymes (Fig. 4g)²¹. Finally, when newly synthesized NOX2 was metabolically labelled with [³⁵S]methionine, higher NOX2 levels were already evident as early as the end of 1-h pulse period (time 0) and a slower decay of NOX2 persisted for up to 4 h during the chase period in NRROS-deficient BMDMs (Fig. 4h). This increased NOX2 was Endo H sensitive (Extended Data Fig. 8f), demonstrating its ER origin. In

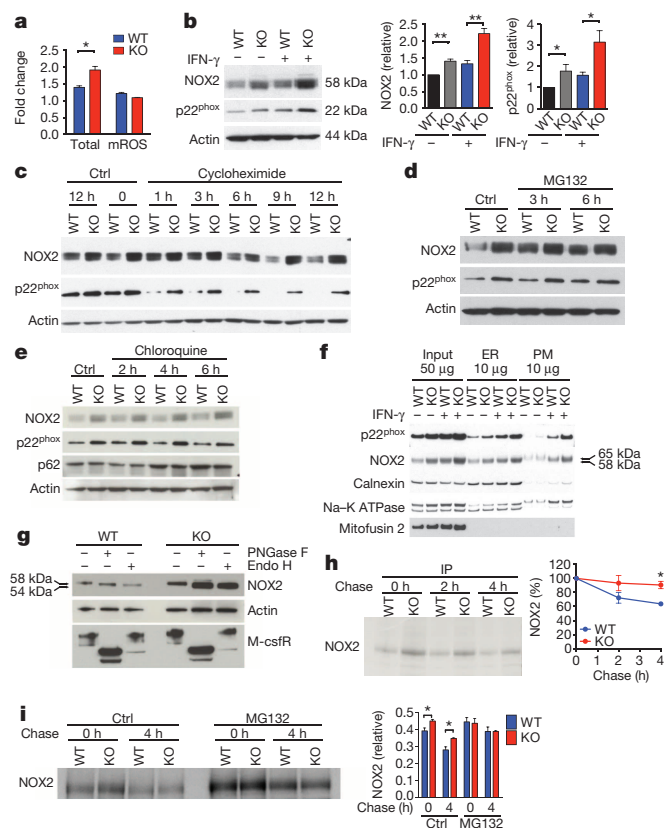


Figure 4 | NRROS regulates the activity of NOX2 oxidase complex in BMDMs. **a,** Zymosan-induced total ROS and mitochondrial ROS (mROS) in IFN- γ -primed WT and NRROS-deficient (KO) BMDMs. Fold change relative to unstimulated control. **b,** Left, NOX2 and p22^{phox} in unprimed (-) and IFN- γ -primed (+) BMDMs. Actin was used as loading control. Right, densitometry analyses relative to actin ($n = 4$). **c-e,** NOX2 and p22^{phox} in IFN- γ -primed BMDMs treated with cycloheximide (**c**), MG132 (**d**) or chloroquine (**e**). **f,** Subcellular fractionation and blotting of unprimed (-) and IFN- γ -primed (+) BMDMs. PM, plasma membrane. **g,** NOX2 in PNGase- or Endo H-treated IFN- γ -primed BMDM lysates. M-CSFR was used as control for Endo H resistance. Actin was used as loading control. **h, i,** Left, autoradiography of immunoprecipitated (IP) NOX2 from [³⁵S]methionine-labelled IFN- γ -primed BMDMs without (**h**) or with (**i**) MG132 treatment. Right, densitometry analyses relative to control in the flow-through with (**h**) or without (**i**) normalization to 0 h samples ($n = 3$). Error bars, s.e.m. * $P < 0.05$, ** $P < 0.01$ (unpaired Student's *t*-test). Data are representative of two (**a, g**) and at least three (**b-f, h-i**) independent experiments.

addition, the difference in protein degradation was abrogated when cells were treated with MG132 (Fig. 4i), suggesting that NRROS facilitated the degradation of nascent NOX2 through the ERAD pathway in phagocytes.

Consistent with these results, we demonstrated that NRROS mostly resided in the ER by subcellular fractionation, flow cytometric analysis and immunofluorescent staining (Fig. 5a and Extended Data Fig. 8g, h). Recent studies have suggested that the heat shock protein (HSP)70-HSP90-CHIP axis is involved in the degradation of NOX2 through ERAD^{19,22}. However, expression of HSP70, HSP90 and CHIP were comparable between wild-type and NRROS-deficient macrophages (Extended Data Fig. 9a). Even though pre-treatment with the HSP90 inhibitor radicicol markedly inhibited NOX2 expression in both wild-type and NRROS-deficient cells—almost to a level where the difference in ROS production between wild-type and NRROS-deficient BMDMs was no longer observed (Extended Data Fig. 9b, c)—the higher NOX2 levels in NRROS-deficient BMDMs were maintained (Extended Data Fig. 9d). These data suggested that NRROS most likely controls NOX2 degradation in the ER by a different mechanism, although we could not exclude a possible cooperation with the HSP90-HSP70-CHIP axis.

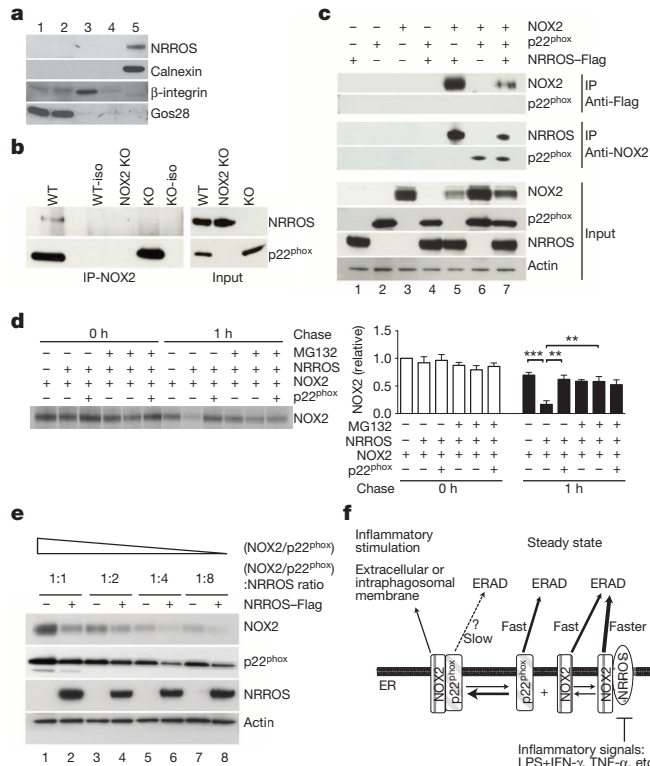


Figure 5 | NRROS promotes NOX2 degradation in the ER. **a**, Subcellular fractionation of RAW cells and western blot analysis. Numbers represent fractions. **b**, Anti-NOX2-immunoprecipitated NRROS and p22^{phox} from IFN-γ-primed BMDMs. iso, isotype control. **c**, NRROS-Flag, NOX2 and p22^{phox} immunoprecipitated with Flag or NOX2 antibody from CHO cells transfected with the indicated plasmids. Bottom panels, input samples. Actin was used as loading control. Numbers below indicate lanes. **d**, Autoradiography of NOX2 from [³⁵S]methionine-labelled, MG132-treated 293T cells transfected with the indicated plasmids. Right graph, densitometry relative to time 0 of cells transfected with NOX2 alone. **e**, NOX2 and p22^{phox} in CHO cells transfected with the indicated ratio of NOX2/p22^{phox} (1:1)-expressing plasmids to NRROS-Flag-expressing plasmid. Actin was used as loading control. Numbers below indicate lanes. **f**, Model depicting NOX2 complex regulation by NRROS. **P < 0.01, ***P < 0.001 (unpaired Student's t-test). Data are representative of at least three independent experiments.

Next, given their colocalization in the ER, we examined whether NRROS interacts with the NOX2-p22^{phox} complex. Interestingly, coimmunoprecipitation of NRROS by NOX2 was detected in wild-type BMDMs (Fig. 5b). As neither the NOX2 nor the p22^{phox} monomer is stable in primary phagocytes, we further studied their interaction with NRROS in CHO and 293T cells²³. Surprisingly, upon ectopic overexpression of Flag-tagged NRROS, together with NOX2 and/or p22^{phox} in CHO cells, we observed a specific interaction between NRROS and NOX2 only, and not between NRROS and the p22^{phox} monomer or the NOX2-p22^{phox} heterodimer (Fig. 5c, lanes 5–7, top panel). On the other hand, NOX2 could form a heterodimer with either NRROS or p22^{phox} (Fig. 5c, lanes 5–7, middle panel). Importantly, p22^{phox} interfered with the interaction between NRROS and NOX2 (Fig. 5c, lanes 5 and 7, top and middle panels). Co-expression of NOX2 with NRROS led to a substantial downregulation of NOX2 protein (Fig. 5c, lanes 3 and 5, bottom panel), but not the transcript (data not shown). The expression of p22^{phox} protein remained unchanged or was only mildly reduced upon NRROS co-expression (Fig. 5c, lanes 2 and 4, bottom panel). Consistent with the co-immunoprecipitation data, the formation of a NOX2-p22^{phox} heterodimer prevented the NRROS-mediated downregulation of NOX2 (Fig. 5c, lanes 5 and 7, bottom panels). Similar results were also obtained in 293T cells (data not shown). Pulse chase experiments in 293T cells further suggested that NRROS facilitated the degradation of NOX2

through the ERAD pathway, which could be prevented either by MG132 treatment or co-expression of p22^{phox} (Fig. 5d). Finally, a relatively stable NOX2-p22^{phox} complex could be shifted to the NRROS-mediated degradation pathway with increased molar ratio of NRROS to NOX2-p22^{phox}, where in addition to the decline in NOX2 levels, a reduction in p22^{phox} levels was observed as well (Fig. 5e, lanes 5 to 8).

Altogether, our data support a model in which NRROS directly interacts with nascent NOX2 monomers and facilitates their degradation through the ERAD pathway (Fig. 5f)²⁴. p22^{phox} competes with NRROS to form a much more stable NOX2-p22^{phox} complex. Certain inflammatory signals can regulate the expression of NRROS, and thereby modulate the expression of the NOX2 complex and ROS production (Fig. 5f). The delicate regulation of NOX2 by NRROS ensures that there is sufficient ROS production by phagocytes during host defence while at the same time limiting collateral tissue damage. Further understanding of this pathway may provide novel therapeutic approaches to target ROS production in various diseases.

METHODS SUMMARY

All animal experiments were approved by the Genentech Institutional Animal Care and Use Committee (IACUC). Mice were infected with *L. monocytogenes* and monitored for mortality or euthanized for bacterial burden analyses. EAE was induced by immunizing mice with MOG_{35–55}-CFA/pertussis toxin and monitored for clinical score and mortality. Oxidative damage in the CNS of EAE-induced mice was assessed by malondialdehyde measurement with ELISA or western blot (OxiSelect MDA kit, Cell Biolabs). *In vivo* ROS neutralization was achieved by injecting mice with a cocktail of scavengers (15 mg kg⁻¹ EUK134 (Cayman Chemical), 20 mg kg⁻¹ FeTPPS (Calbiochem) and 50 mg kg⁻¹ PBN (Sigma-Aldrich)). *In vitro* *E. coli* killing was assessed by gentamicin protection assay. *In vitro*, ROS was measured by incubating primed phagocytes with an inducing agent and either luminol for continuous detection by luminometer or CM-H₂DCFDA (total ROS) or MitoSOX (mROS) (Invitrogen) for FACS analyses. *Ex vivo* ROS was measured by incubating cells with CM-H₂DCFDA and analysed by FACS. Whole cell/tissue lysates prepared in RIPA or Triton X-100 buffer were used for immunoprecipitation and western blot studies. Metabolic labelling of cells was performed using [³⁵S]methionine. Subcellular fractionation was carried out by sucrose gradient ultracentrifugation. Total RNA was used in microarray or Taqman expression analyses.

Online Content Any additional Methods, Extended Data display items and Source Data are available in the online version of the paper; references unique to these sections appear only in the online paper.

Received 14 December 2012; accepted 14 February 2014.

Published online 13 April 2014.

1. Bedard, K. & Krause, K. H. The NOX family of ROS-generating NADPH oxidases: physiology and pathophysiology. *Physiol. Rev.* **87**, 245–313 (2007).
2. Lambeth, J. D. NOX enzymes and the biology of reactive oxygen. *Nature Rev. Immunol.* **4**, 181–189 (2004).
3. West, A. P. et al. TLR signalling augments macrophage bactericidal activity through mitochondrial ROS. *Nature* **472**, 476–480 (2011).
4. Honda, F. et al. The kinase Btk negatively regulates the production of reactive oxygen species and stimulation-induced apoptosis in human neutrophils. *Nature Immunol.* **13**, 369–378 (2012).
5. Wang, G. et al. Cutting edge: Slamf8 is a negative regulator of Nox2 activity in macrophages. *J. Immunol.* **188**, 5829–5832 (2012).
6. Di, A. et al. The redox-sensitive cation channel TRPM2 modulates phagocyte ROS production and inflammation. *Nature Immunol.* **13**, 29–34 (2012).
7. McPhail, L. C., Clayton, C. C. & Snyderman, R. The NADPH oxidase of human polymorphonuclear leukocytes. Evidence for regulation by multiple signals. *J. Biol. Chem.* **259**, 5768–5775 (1984).
8. El-Benna, J., Dang, P. M. & Gougerot-Pocidalo, M. A. Priming of the neutrophil NADPH oxidase activation: role of p47^{phox} phosphorylation and NOX2 mobilization to the plasma membrane. *Semin. Immunopathol.* **30**, 279–289 (2008).
9. Anrather, J., Racchumi, G. & Iadecola, C. NF-κB regulates phagocytic NADPH oxidase by inducing the expression of gp91^{phox}. *J. Biol. Chem.* **281**, 5657–5667 (2006).
10. Dinauer, M. C., Deck, M. B. & Unanue, E. R. Mice lacking reduced nicotinamide adenine dinucleotide phosphate oxidase activity show increased susceptibility to early infection with *Listeria monocytogenes*. *J. Immunol.* **158**, 5581–5583 (1997).
11. Shiloh, M. U. et al. Phenotype of mice and macrophages deficient in both phagocyte oxidase and inducible nitric oxide synthase. *Immunity* **10**, 29–38 (1999).
12. Nikolic, I. et al. A reversible form of axon damage in experimental autoimmune encephalomyelitis and multiple sclerosis. *Nature Med.* **17**, 495–499 (2011).

13. Tse, H. M. *et al.* NADPH oxidase deficiency regulates Th lineage commitment and modulates autoimmunity. *J. Immunol.* **185**, 5247–5258 (2010).
14. Ouyang, W., Kolls, J. K. & Zheng, Y. The biological functions of T helper 17 cell effector cytokines in inflammation. *Immunity* **28**, 454–467 (2008).
15. Wållberg, M., Bergquist, J., Achour, A., Breij, E. & Harris, R. A. Malondialdehyde modification of myelin oligodendrocyte glycoprotein leads to increased immunogenicity and encephalitogenicity. *Eur. J. Immunol.* **37**, 1986–1995 (2007).
16. Sheppard, F. R. *et al.* Structural organization of the neutrophil NADPH oxidase: phosphorylation and translocation during priming and activation. *J. Leukoc. Biol.* **78**, 1025–1042 (2005).
17. DeLeo, F. R. *et al.* Processing and maturation of flavocytochrome b558 include incorporation of heme as a prerequisite for heterodimer assembly. *J. Biol. Chem.* **275**, 13986–13993 (2000).
18. Parkos, C. A., Dinauer, M. C., Jesaitis, A. J., Orkin, S. H. & Curnutte, J. T. Absence of both the 91kD and 22kD subunits of human neutrophil cytochrome b in two genetic forms of chronic granulomatous disease. *Blood* **73**, 1416–1420 (1989).
19. Chen, F. *et al.* Hsp90 regulates NADPH oxidase activity and is necessary for superoxide but not hydrogen peroxide production. *Antioxid. Redox Signal.* **14**, 2107–2119 (2011).
20. Pollock, J. D. *et al.* Mouse model of X-linked chronic granulomatous disease, an inherited defect in phagocyte superoxide production. *Nature Genet.* **9**, 202–209 (1995).
21. Lewis, V. *et al.* Glycoproteins of the lysosomal membrane. *J. Cell Biol.* **100**, 1839–1847 (1985).
22. Chen, F. *et al.* Opposing actions of heat shock protein 90 and 70 regulate nicotinamide adenine dinucleotide phosphate oxidase stability and reactive oxygen species production. *Arterioscler. Thromb. Vasc. Biol.* **32**, 2989–2999 (2012).
23. Casbon, A. J., Allen, L. A., Dunn, K. W. & Dinauer, M. C. Macrophage NADPH oxidase flavocytochrome B localizes to the plasma membrane and Rab11-positive recycling endosomes. *J. Immunol.* **182**, 2325–2339 (2009).
24. Brodsky, J. L. Cleaning up: ER-associated degradation to the rescue. *Cell* **151**, 1163–1167 (2012).

Supplementary Information is available in the online version of the paper.

Acknowledgements We thank D. Seshasayee and H. Van Gorp for providing L929 condition media; J. Tao for helping with the screening of NRROS antibodies; C. Kuijl, J. R. Junutula (Genentech) and D. Monack (Stanford University) for providing *S. typhimurium*; W. Lee for providing *L. monocytogenes* and K. Huynh for providing dsRed *E.coli*; W. Forrest (Genentech) for help with statistical analysis; M. Roose-Girma, M. Schlatter and J. Aurellano (Genentech) for help with design and generation of Nrros conditional knockout construct and ES cells.

Author Contributions W.O. and R.N. devised the project and wrote the manuscript. R.N. designed and performed most of the experiments. K.W. contributed to Fig. 2h and Extended Data Figs 1e, 2a, b, N.O. contributed to Fig. 2f, S.R. contributed to Fig. 3a–g, C.E. contributed to Extended Data Fig. 5c–g, P.A.V. contributed to Extended Data Table 1, R.L. contributed to Fig. 5c, d. K.W., N.O., S.R. and C.E. helped to edit the manuscript. J.D. made the constructs used in Fig. 5 and Extended Data Fig. 8g, h. I.P. and J.D.V. contributed to EAE experiments in Fig. 3a, b, g and Extended Data Fig. 5c, f. A.S. and T.S. assisted in generating NRROS-specific antibodies (Fig. 1b and Extended Data Fig. 1c, e, h–j). P.C. carried out histopathology analyses and contributed to Extended Data Fig. 5d, e, g. R.H.S. and Z.M. assisted in microarray analysis and J.H. performed bioinformatics analysis (Extended Data Fig. 1a).

Author Information Reprints and permissions information is available at www.nature.com/reprints. The authors declare competing financial interests: details are available in the online version of the paper. Readers are welcome to comment on the online version of the paper. Correspondence and requests for materials should be addressed to W.O. (ouyangwenjun@gene.com).

METHODS

Mice. NRROS-deficient mice were generated in collaboration with Lexicon Pharmaceuticals²⁵ and backcrossed to C57BL/6J more than 14 generations. NOX2-deficient mice were procured from Jackson Laboratories and bred with NRROS-deficient mice to generate NRROS NOX2 double-deficient mice. NRROS conditional knockout (*Nrrs*^{fl/fl}) mice were generated in-house by targeting exon 4 of *Nrrs* that encodes most of the protein. These floxed mice were bred with LysM-Cre mice (kind gift from University of California, San Diego) to specifically delete NRROS expression in M lysozyme-expressing cells, namely macrophages, monocytes and neutrophils. Mice were routinely genotyped by PCR using the following primers: 5'-TACTCACTGGCCTTGCCCTC-3', 5'-AGAGTTCCATCCTCAGTCCC-3' and 5'-GTTCACATCTGGTGCCAGAC-3'. C57BL/6J and B6.SJL-Ptprc^aPepc^b/BoyJ mice were procured from Jackson Laboratories. *Rag2*-deficient mice (B6.129S6-*Rag2tm1Ifwa* N12) were obtained from Taconic.

For the generation of bone marrow chimaeras, B6.SJL-Ptprc^aPepc^b/BoyJ recipient mice were irradiated with a total of 1,050 rads (in two doses of 525 rads separated by 4-h interval) using a ¹³⁷Cs source. 10–15 × 10⁶ total bone marrow cells isolated from femur and tibias of the wild-type and NRROS-deficient donor mice were injected into the tail vein. Reconstituted mice were given water containing 0.11 mg ml⁻¹ polymyxin B and 1.1 mg ml⁻¹ neomycin for 2 weeks and then switched to regular water. Mice were allowed to reconstitute for at least 12 weeks (more than 90% reconstitution as assessed by CD45.1 (A20, catalogue no. 553776) and CD45.2 antibody (104, catalogue no. 558702) (BD Biosciences) staining and FACS (LSR II, BD Biosciences)) and used for *in vivo* experiments. All animal experiments were approved by the Genentech Institutional Animal Care and Use Committee.

Isolation of cells. For BMDMs, femur and tibia were collected from 3–5 mice of each genotype and bone marrow cells were flushed with complete DMEM containing 50 U ml⁻¹ penicillin, 50 mg ml⁻¹ streptomycin, 2 mM L-glutamine, sodium pyruvate and 10% FBS. Erythrocytes were removed by ACK red blood cell lysis buffer treatment and the cell suspension was filtered through a 70-μm cell strainer to remove any cell clumps. The single-cell suspensions were then cultured at 37 °C for 1 h, and non-adherent cells were collected and re-plated in complete DMEM with 20% L929 conditioned media. To fully differentiate BMDMs, the cells were cultured for an additional 6 days with media change every 3 days. All the cells, when analysed by FACS, were CD11b⁺F4/80⁺ (BD Biosciences). In some experiments, recombinant mouse M-CSF (R&D Systems) was used at a concentration of 50 ng ml⁻¹ instead of L929 medium. BMDMs were primed with 10 ng ml⁻¹ of IFN-γ (R&D Systems) for 18–24 h, unless otherwise stated.

For peritoneal macrophages, mice were injected with 1 ml of 4% thioglycollate, and 4 days later peritoneal cells were collected by lavage using 8 ml PBS. Cells were allowed to adhere for at least 2 h and adherent macrophages were collected, counted and plated in complete DMEM for further analysis.

For neutrophil isolation, single-cell suspensions of the total bone marrow cells from 3–4 mice were prepared and subjected to Percoll gradient separation (78–69%–52%) by centrifugation at 1,500g for 40 min. Neutrophils were collected from 78–69% interphase, washed twice, re-suspended in HBSS and used for further analysis. Cell purity was more than 90% as analysed by FACS staining with CD11b (M1/70, catalogue no. 48-0112; eBioscience) and Gr-1 antibodies (RB6-8C5, catalogue no. 553126; BD biosciences).

For studies with human cells, blood received at Genentech health centre from healthy donors was used to isolate peripheral blood mononuclear cells (PBMCs) by Ficoll gradient (GE Healthcare). Monocytes were further isolated from the PBMCs using human monocyte isolation kit II (Miltenyi Biotech) according to the manufacturer's instructions. Monocyte-derived macrophages were generated by culturing the purified monocytes for 7 days in complete RPMI 1640 containing 10% FBS and 100 ng ml⁻¹ human M-CSF (R&D Systems). Fresh medium containing 100 ng ml⁻¹ of M-CSF was added to cells on day 4 and cells were used for further analysis on day 7. PBMCs were also used to isolate B cells and T cells using CD19 microbeads and Pan T Cell Isolation Kit II (Miltenyi Biotech), respectively, according to the manufacturer's instructions.

Isolation of CNS-infiltrating mononuclear cells. Animals were perfused with 30 ml of PBS, and brain and spinal cords were collected. A single-cell suspension was obtained by grinding the tissues using 1 ml syringe plunger and passed through a 70-μm strainer. Mononuclear cells were obtained by Percoll gradient (37/70%, GE Healthcare) centrifugation at 390g for 30 min at room temperature (20–25 °C) collected from the interphase, washed and used for further analysis.

Plasmids. Sequence coding murine NRROS protein was amplified by PCR using mouse splenic complementary DNA as template, and inserted into BglII(blunt)/EcoRI site of Nflag-pPRK vector which has signal peptide sequence and Flag-tag sequence. Then, cDNA encoding signal peptide–Flag-tag–NRROS was transferred onto retroviral vector pMSCV-IRES-GFP to generate Flag-NRROS-pMSCV. This amino-terminally Flag-tagged NRROS (Flag-NRROS) was used to generate RAW stable cell lines. A plasmid expressing carboxy-terminally Flag-tagged NRROS

(NRROS–Flag) was generated by cloning PCR-amplified coding region of NRROS including its signal sequence into pRK5 vector using Ascl and XbaI sites to generate NRROS–Flag-pRK. Mouse *Cyba* and *Cybb* genes encoding p22^{phox} and NOX2, respectively, were amplified by PCR using mouse splenic cDNA and cloned into pRK5 vector using EcoRI and XbaI sites to generate p22^{phox}-pRK and NOX2-pRK, respectively.

Generation of Flag-NRROS-RAW cells by retroviral transduction. Phoenix E cells were transfected with either Flag-NRROS-pMSCV or pMSCV-IRES-GFP control plasmid by the calcium phosphate method. After 48 h, the retroviral supernatants were collected, filtered through 0.45-μm filters, supplemented with polybrene (10 μg ml⁻¹) and added to RAW cells that were plated in a six-well plate the previous night. Plates were centrifuged at 1,200g at 32 °C for 120 min. The viral supernatant was replaced by complete DMEM after an additional 2 h. Transduced RAW cells were sorted (FACSAria, BD Biosciences) based on GFP expression.

Transfection of cells. CHO cells were transfected with the indicated plasmid using Lipofectamine 2000 (Life Technologies) according to manufacturer's instructions. In brief, 10 μg total DNA was diluted in 500 μl of opti-MEM and 25 μl of Lipofectamine 2000 was diluted in another 500 μl of opti-MEM. The two were combined, incubated for 20 min and added drop-wise to cells grown on 100-mm plates at 70–80% confluence. After 24 h, cells were collected by trypsinization and lysed in RIPA buffer (50 mM Tris, pH 7.4, 150 mM NaCl, 2 mM EDTA, 1% NP-40, 1% SDS) and subjected to western blot analysis or were used for immunoprecipitation with the indicated antibody. For the titration experiments, 2.5 μg each of NOX2-pRK and p22^{phox}-pRK plasmids were mixed and then serially diluted two-fold while maintaining their 1:1 ratio. The amount of NRROS–Flag-pRK plasmid was held constant at 2.5 μg and added to the above tubes so that the ratio of NOX2-pRK:p22^{phox}-pRK:NRROS–Flag-pRK was 1:1:1, 1:1:2, 1:1:4 and 1:1:8. Total amount of DNA was adjusted to 10 μg with empty pRK plasmid. After 24 h cells were collected, lysed and subjected to western blot analyses. 293T cells grown in 100-mm plates were transfected using Fugene 6 reagent (Promega) at 3:1 ratio (DNA:Fugene), according to the manufacturer's instructions and processed as described for CHO cells. Both CHO and 293T cells were obtained from an internal cell-banking program (gCell) at Genentech.

siRNA knockdown. Chemically modified siRNAs²⁶ were synthesized in house. siRNA specific for *Nrrs* was composed of 5'-mAmGAGCUAGAUUUGCAGAdGdAdAmAmCmU-3' (sense) and 5'-dTUUUCUCUGCAAUCUAGCmUmCmU-3' (antisense), and the control scrambled siRNA was 5'-mGmGAGCGCACCAU CUUCdCdAmAmUmU-3' (sense) and 5'-dTUGAGAAGAUGGUGGCmUmCm-3' (antisense). RAW cells were transfected with ~600 pmol siRNA using Cell Line Nucleofection Kit V (Lonza). 24 h later, cells were re-plated at 5 × 10⁴ cells per well of a 96-well clear-bottom white plate (Corning), primed with 10 ng ml⁻¹ IFN-γ (R&D Systems) for another 24 h and used for further analysis.

ROS measurement. For luminol-based ROS measurement, 1 × 10⁵ macrophages were plated in clear-bottomed 96-well white plates (Corning) in triplicate, and primed for 24 h with 10 ng ml⁻¹ of IFN-γ, 100 ng ml⁻¹ LPS (Invivogen) or 100 ng ml⁻¹ TNF-α (R&D Systems), either alone or in combination. In most of the experiments, cells were primed with 10 ng ml⁻¹ IFN-γ unless otherwise indicated. Oxidative burst was induced in luminol medium (PBS containing 5 mM glucose, 1 mM MgCl₂, 0.5 mM CaCl₂ and 100 μM luminol (Sigma-Aldrich)) by stimulating macrophages with 100 μg ml⁻¹ zymosan A (Invivogen), 100 ng ml⁻¹ PMA (Sigma-Aldrich), heat-killed *Listeria monocytogenes* (Invivogen) at multiplicity of infection (m.o.i.) 50, *E. coli* strain 26 (ATCC) at m.o.i. 50, or *S. typhimurium* SL1344 (a kind gift from D. Monack, Stanford University) at m.o.i. 10. Luminescence was measured by Glomax luminometer (Promega). Neutrophils and CNS mononuclear cells were re-suspended in the luminol medium (1 × 10⁵ cells per well) and stimulated with 100 ng ml⁻¹ PMA or 100 μg ml⁻¹ zymosan. For experiments with inhibitors, the following chemicals were added to the cell cultures during the last 1 h of the priming: 5 μM diphenyleneiodonium (Calbiochem), 20 μM antimycin A (Sigma-Aldrich) or 3 mM apocynin (Calbiochem) unless otherwise indicated. For treatment with apocynin, the compound continued to be present during the stimulation, whereas for other treatments, cells were washed with PBS before ROS induction.

For FACS-based measurements, macrophages plated in 6-well plates were treated with the indicated stimulant for 30 min at 37 °C in the presence or absence of 5 μM CM-H₂DCFDA (Invitrogen) to measure total intracellular ROS or 5 μM MitoSOX (Invitrogen) to measure mitochondrial ROS. Cells were washed with PBS, collected by trypsinization and analysed by FACS. For ROS measurement induced by rotenone (Calbiochem) or antimycin A, cells were treated with or without 10 μM of the compounds for 2 h, washed with PBS, collected by trypsinization and analysed by FACS. Splenocytes and CNS mononuclear cells were stimulated with 100 ng ml⁻¹ PMA in the presence or absence of 5 μM CM-H₂DCFDA for 30 min, washed with PBS, collected and stained for surface markers CD11b (eBioscience), Gr-1, B220 and CD3 (BD Biosciences) for 30 min on ice before analysing by FACS.

Measurement of nitric oxide. BMDMs were treated with 10 ng ml⁻¹ IFN- γ , 10 ng ml⁻¹ TNF- α , 100 ng ml⁻¹ LPS or their combination for 24 h, and nitric oxide in the culture supernatant was measured using Griess assay (Promega) with Spectra Max 340 (Molecular Devices) spectrophotometer according to the manufacturer's recommendations.

RNA isolation and real-time RT-PCR. RNA was isolated using RNeasy kit (Qiagen). Total RNA of 20 different human tissues was obtained from Clontech. Mouse major tissues total RNA was procured from ZymoGen. RNA samples were analysed by real-time RT-PCR with TaqMan One-Step RT-PCR Master Mix reagents (Applied Biosystems) and the appropriate primers and probes. Results were normalized to those of the housekeeping gene *Rpl19* (encoding ribosomal protein L19) and are reported as 2^{ΔCT}. The primer and probe sets used were: *Rpl19*: forward 5'-GCATCCTCATGGAGCACAT-3', reverse 5'-CTGGTCAGGCCAGGAGCTT-3', probe 5'-CTTGCAGGGCTTGTCTGCCTT-3'; *Nrrs*: forward 5'-ACTGCAGC TTCCAAGGA-3', reverse 5'-TGGGTACCGAAGCAAGGT-3', probe 5'-AGT CAGCGACTCCGTCGACCAC-3'; *Cybb* (NOX2): forward 5'- ACTGCGGAGA GTTTGAAGA-3', reverse 5'-GGTGATGACCACCTTTGCT-3', probe 5'-GA GGTGTTGCGTTTGGCA-3'; and *Cyba* (p22^{phox}): forward 5'-AAAGAGG AAAAAGGGTCCA-3', reverse 5'-ATGGCTGCCAGCAGATAGAT-3', probe 5'-ACTACGTCCGGCTGCCCTC-3'.

Microarray analysis. Statistical analyses of microarray data were performed using the R programming language (<http://r-project.org>). Microarray data were normalized using the RMA method²⁷. Data were prefiltered to remove probes that were not mapped to an annotated Entrez gene. We also filtered our data to retain only a single probe per gene, selecting the probe with the highest variance, if multiple probes were found for the gene²⁸. For differential expression analysis, the limma R package was used²⁹. We modelled the synergistic regulation of gene expression by the combined IFN- γ and LPS treatment as an interaction term in our linear model. This model will identify changes that are significantly different from the sum of the individual treatments. Multiple test correction was done using the method of Benjamini and Hochberg³⁰. Genes were considered significantly different if they changed more than 1.4-fold at a false discovery rate of 0.05. Genes were further filtered for immune-cell-specific expression using the gene sets defined by the Immune Response In Silico (IRIS) project³¹. As the IRIS-defined gene sets were derived from human immune cells, we mapped the human genes to mouse orthologues using the HomoloGene database³². Genes from all IRIS-defined categories were included in the analysis. Data were submitted to the NCBI (accession number GSE53986).

Subcellular fractionation. A discontinuous sucrose gradient was used for fractionation of cells as described³³. In brief, cells were collected either by scraping (RAW cells) or by trypsinization (BMDMs), washed with PBS, re-suspended in isotonic solution (10 mM Tris, pH 7.5, 0.5 mM MgCl₂), incubated on ice for 15 min and homogenized using a Dounce homogenizer. Cell disruption was confirmed by trypan blue staining. Homogenate was made isotonic with 1.46 M sucrose (250 mM final concentration) and centrifuged at 10,000g for 5 min to remove debris and unbroken cells. The homogenate was then layered onto a sucrose gradient of 0.58 M, 0.88 M and 1.1 M, and ultracentrifuged at 100,000g for 2 h using TLS5 (Beckman Coulter optima). Five fractions numbered 1–5 were collected and analysed by western blot. ER and plasma membranes were enriched in the pellet and fraction 3, respectively. Fractions 1 and 2 were enriched in Golgi apparatus and lysosome.

Tissue lysates, immunoprecipitation and western blot analysis. For lysing tissues to analyse NRROS expression, C57BL/6 mice were perfused with 30 ml PBS, organs were collected and homogenized in RIPA buffer containing protease and phosphatase inhibitor cocktail (Halt protease and phosphatase inhibitor cocktail from Pierce). To analyse NRROS expression in different immune cell types, FACS-sorted cells were lysed in RIPA buffer containing protease and phosphatase inhibitor cocktail. For inhibitor treatments in BMDMs, cells were cultured in the presence of cycloheximide (10 μ g ml⁻¹, Sigma), MG132 (10 μ g ml⁻¹, Calbiochem) or chloroquine (10 μ g ml⁻¹, Calbiochem) for the indicated time, collected and lysed in RIPA buffer. Neutrophils were lysed in solution containing 10% glycerol, 3% SDS, 1 mM PMSF and 5 mM NaF, and heated immediately at 95 °C for 5 min. Equal amounts of proteins, measured using BCA assay (Pierce), were separated by SDS-PAGE on 4–12% Bis-Tris gels (Invitrogen) and transferred onto nitrocellulose membranes using iBlot apparatus (Invitrogen). Membranes were blocked for 1 h at room temperature with 5% milk in TBST and probed with indicated antibody in 5% milk overnight at 4 °C.

The following primary antibodies were used: NOX2 (gp91^{phox}) (54.1, catalogue no. sc-130543), p22^{phox} (FL-195, catalogue no. sc-20781), p47^{phox} (D10, catalogue no. sc-17845), p40^{phox} (H-300, catalogue no. sc-30087), GFP (B-2, catalogue no. sc-9996) from Santa Cruz Biotechnology, p67^{phox} (rabbit polyclonal, catalogue no. 07-002) from Millipore, phospho-p40^{phox} (T154, catalogue no. 4311), β -integrin (rabbit polyclonal, catalogue no. 4706), Na-K ATPase- α (rabbit polyclonal, catalogue no. 3010), GAPDH-horseradish peroxidase (HRP) (14C10, catalogue no.

3683), HSP90 (C45G5, catalogue no. 4877), HSP70 (D69, catalogue no. 4876), CHIP (C3B6, catalogue no. 2080) from Cell Signaling Technology, phospho-p47^{phox} (Ser370) (rabbit polyclonal, catalogue no. A1171) from Assay Biotechnology, calnexin (rabbit polyclonal, catalogue no. SPA-860) from Stressgen Biotechnologies, gos28 (rabbit polyclonal, catalogue no. GTX61678) from GeneTex, actin (rabbit polyclonal, catalogue no. A5060) from Sigma-Aldrich. Anti-NRROS monoclonal antibody was generated by immunizing Armenian hamsters with *E. coli*-derived recombinant NRROS (extracellular domain). Secondary antibodies include HRP-conjugated anti-rabbit (catalogue no. 7074), anti-mouse (catalogue no. 7076) (Cell Signaling Technology) and anti-Armenian hamster (Jackson Immunoresearch, catalogue no. 127-035-160). Image quantification was performed using ImageJ software (NIH).

For glycosidase treatment, lysates were incubated with PNGase-F (New England Biolabs) for 1 h or with Endo-H (New England Biolabs) for about 18 h according to the manufacturer's instructions. For NOX2 immunoprecipitation, lysates were incubated with 10 μ g of the antibody overnight at 4 °C, immunoprecipitates were captured with protein A/G ultralink resin (Thermo Scientific) and eluted with sample buffer. For anti-Flag immunoprecipitation, lysates were incubated with EZview Red ANTI-FLAG M2 affinity gel (Sigma) at 4 °C for 4 h and eluted with 3 \times Flag peptide (Sigma) according to manufacturer's instructions.

[³⁵S]Methionine metabolic labelling. Metabolic labelling of BMDMs was performed as described^{34,35}. In brief, BMDMs were primed with IFN- γ (10 ng ml⁻¹) for 24 h. Cells were washed and incubated with 25 μ Ci ml⁻¹ [³⁵S]methionine (Perkin Elmer) in DMEM high glucose medium without methionine (Life Technologies) supplemented with 50 U ml⁻¹ penicillin, 50 mg ml⁻¹ streptomycin, 2 mM L-glutamine, sodium pyruvate and 10% FBS. After 1 h of labelling, cells were either collected (for time 0) or incubated further for the indicated time in complete DMEM with non-radiolabelled methionine.

Cells were washed three times with cold PBS, and then lysed in lysis buffer (50 mM Tris, pH 7.5, 150 mM NaCl, 1 mM EDTA, 1% Triton X-100) containing protease and phosphatase inhibitor cocktail (Halt protease and phosphatase inhibitor cocktail from Pierce). Lysates were pre-cleared with control agarose beads (Pierce) for 1 h and incubated with anti-NOX2 antibody overnight. Immunoprecipitates were captured using Protein A/G ultralink resin, eluted with sample buffer and separated by SDS-PAGE. Gels were dried using a gel drier and exposed to X-ray film.

For experiments with Endo-H digestion, immunoprecipitates were eluted in Endo H buffer (100 mM Na-acetate, pH 5.6, 0.1% SDS, 1 mM PMSF)³⁶. Equal amounts of the eluted samples were incubated with or without Endo-H (New England Biolabs) for about 18 h and samples were used in SDS-PAGE as described above. Densitometry analysis was performed using ImageJ software and data were normalized to a nonspecific band in the input samples.

For experiments using MG132, cells were pre-incubated with 20 μ M MG132 (Calbiochem) for 1 h before pulse. The MG132 treatment was continued during pulse and until end of the chase period.

Metabolic labelling and NOX2 immunoprecipitation in 293T cells was carried as described for BMDMs except that cells were pulsed with 100 μ Ci ml⁻¹ [³⁵S] methionine for 15 min instead of 1 h. Overexpressing NOX2 by transient transfection enabled us to pulse cells for a shorter duration (for example, 15 min) and still be able to immunoprecipitate and detect NOX2.

RAC1 activation assay. The activity of RAC1 in wild-type and NRROS-deficient BMDMs was measured using RAC1 activation assay kit (Cell Biolabs) according to the manufacturer's instructions. In brief, wild-type and NRROS-deficient BMDMs were primed with 10 ng ml⁻¹ IFN- γ for 24 h. Cells were stimulated with 100 μ g ml⁻¹ zymosan for 5, 15 or 30 min. Cell lysates were prepared and used immediately for RAC1 pulldown with the p21-activated protein kinase (PAK)-p21 binding domain (PBD) beads. The activated RAC1 was detected by anti-RAC1 antibody supplied with the kit.

Immunofluorescence staining. RAW 264.7 cells stably expressing Flag-NRROS were grown overnight in chamber slides. Cells were then fixed with 4% paraformaldehyde, washed with PBS, and treated with 50 mM NH₄Cl/PBS. After rinsing with PBS, cells were permeabilized and blocked in saponin buffer (0.4% Saponin, 1% BSA, 2% normal goat serum in PBS). Mouse anti-Flag (Sigma-Aldrich), rabbit anti-calnexin (Enzo Life Sciences) and rat anti-LAMP1 (Santa Cruz Biotechnology) antibodies were used. Secondary goat anti-mouse Alexa 647 was purchased from Invitrogen and goat anti-rabbit-Cy3 and donkey anti-rat-Cy5 antibodies were from Jackson Immunoresearch.

Confocal microscopy. Images were captured by a Leica SPE laser scanning confocal microscope (Leica) equipped with Leica DM5500Q under 63 \times 1.30 NA CS ACS APO oil-immersion objective controlled by LAS AF image acquisition and processing software. Excitation and emission for DAPI, Alexa 488, Cy3 and Cy5 were used at default settings set by the manufacturer (Leica).

Phagocytosis assay. dsRed *E. coli* (gift from K. Huynh, Genentech) were opsonized with fresh mouse serum, and BMDMs primed with 10 ng ml⁻¹ IFN- γ for

24 h were allowed to phagocytose the bacteria for 30 min. Cells were collected and analysed by FACS.

In vitro bacterial killing assay. Macrophages plated at 0.25×10^6 cells per well of a 24-well plate were primed with 10 ng ml^{-1} of IFN- γ for 24 h in antibiotics-free complete DMEM. Cells were infected with serum opsonized *E. coli* strain 26 at m.o.i. of 50 in 250 μl total volume by centrifugation at room temperature for 5 min at 1,000 r.p.m. to synchronize the infection and further incubated at 37°C for 30 min. Medium was replaced with $100 \text{ }\mu\text{g ml}^{-1}$ of gentamicin (Invitrogen)-containing medium. After an additional 5 min (considered as 30-min time point), 30 min (60-min time point) and 90 min (120-min time point), cells were washed twice with 1 ml PBS and lysed in 250 μl of 0.1% Triton X-100 in PBS. Twofold serial dilutions of the lysates were prepared in PBS and 5 μl was dropped on a LB agar plate with no antibiotics. Colonies were counted after 18–24 h incubation at 37°C . Total protein in the lysates was measured using BCA assay and the colony numbers were normalized to the amount of protein.

Neutrophil bacterial killing assay was performed as described previously³⁷. In brief, twofold dilutions ($2.5\text{--}0.625 \times 10^6$) of neutrophils were added to 25×10^6 c.f.u. *E. coli* strain 26 and fresh mouse serum (5% final concentration) in a total volume of 1 ml, in triplicate. The tubes were rotated for 2 h and 100 μl of the sample was diluted with 1 ml sterile distilled water (pH adjusted to 11 by NaOH) to lyse cells. Serial dilutions were prepared and plated on LB agar plates without antibiotics. Bacterial colonies were counted after 24 h incubation at 37°C .

In vivo bacterial challenge. For *L. monocytogenes* infection studies, age- and sex-matched (6–8 weeks old) wild-type, NRROS-deficient, NOX2-deficient or NRROS NOX2 double-deficient littermate mice were administered intravenously with *L. monocytogenes* (ATCC 43251) (0.1×10^6 c.f.u. for females and 0.5×10^6 c.f.u. for males), and were monitored for 14 days for morbidity and mortality. For bacterial burden experiments, mice were administered intravenously with 1×10^6 c.f.u. *L. monocytogenes* or 2×10^8 c.f.u. *E. coli* strain 26, and killed at 48 h (*L. monocytogenes*) or 6 h (*E. coli*). Spleens and livers were collected in 50-ml tissue grinder tubes (VWR International) and homogenized in 0.1% Triton X-100 in PBS. Twofold serial dilutions of the homogenates were prepared and plated in triplicate on brain heart infusion agar. Bacterial colonies were counted after 24 h. Total protein in the lysate was measured using BCA assay and colony numbers were normalized to the amount of protein.

For ROS neutralization, mice were injected intravenously with either a cocktail of scavengers³⁸ that included 15 mg kg^{-1} EUK134 (Cayman chemicals) 20 mg kg^{-1} FeTPPS (5,10,15,20-tetrakis(4-sulphonatophenyl)porphyrinato iron (III) chloride) (Calbiochem) and 50 mg kg^{-1} PBN (*N*-tert-butyl- α -phenylnitronite) (Sigma-Aldrich) or 2.5% DMSO (Sigma-Aldrich) as vehicle control in a total volume of 200 μl at 60 min before administering *L. monocytogenes*. The spleens and livers were collected after 24 h and processed as described above, for enumeration of bacterial burden.

For all *L. monocytogenes* infection experiments, a sample size of at least five mice per genotype was used in each independent experiment except for data in Fig. 2*i,j* where three mice were used for some groups. Mice of both genders were used. No animals were excluded from any study. No blinding or randomization method was used to group the animals.

Induction of EAE. EAE was induced as described previously³⁹. In brief, age- and sex-matched littermate mice were immunized subcutaneously at the base of the tail with 300 μg MOG_{35–55} peptide emulsified in 800 μg *Mycobacterium tuberculosis*-supplemented CFA (Difco Laboratories). On day 0 and day 2 post-immunization, 200 ng pertussis toxin (List Biologicals) was administered intraperitoneally. Clinical disease was scored daily starting on day 8 until day 30 as follows: 0, no clinical disease; 1, limp tail or hind limb weakness but not both; 2, limp tail and hind limb weakness; 3, partial hind limb paralysis; 4, complete hind limb paralysis; 5, moribund/death.

For ROS neutralization, a cocktail of scavengers was used as described previously³⁸. In brief, mice were administered intraperitoneally every 12 h with the aforementioned cocktail or vehicle control starting from day 9 or day 10 post-immunization depending on the appearance of first clinical signs.

All the mice used for EAE experiments shown in Fig. 3 were bone marrow chimaeric mice. The chimaeric mice were generated when they were around 6 weeks

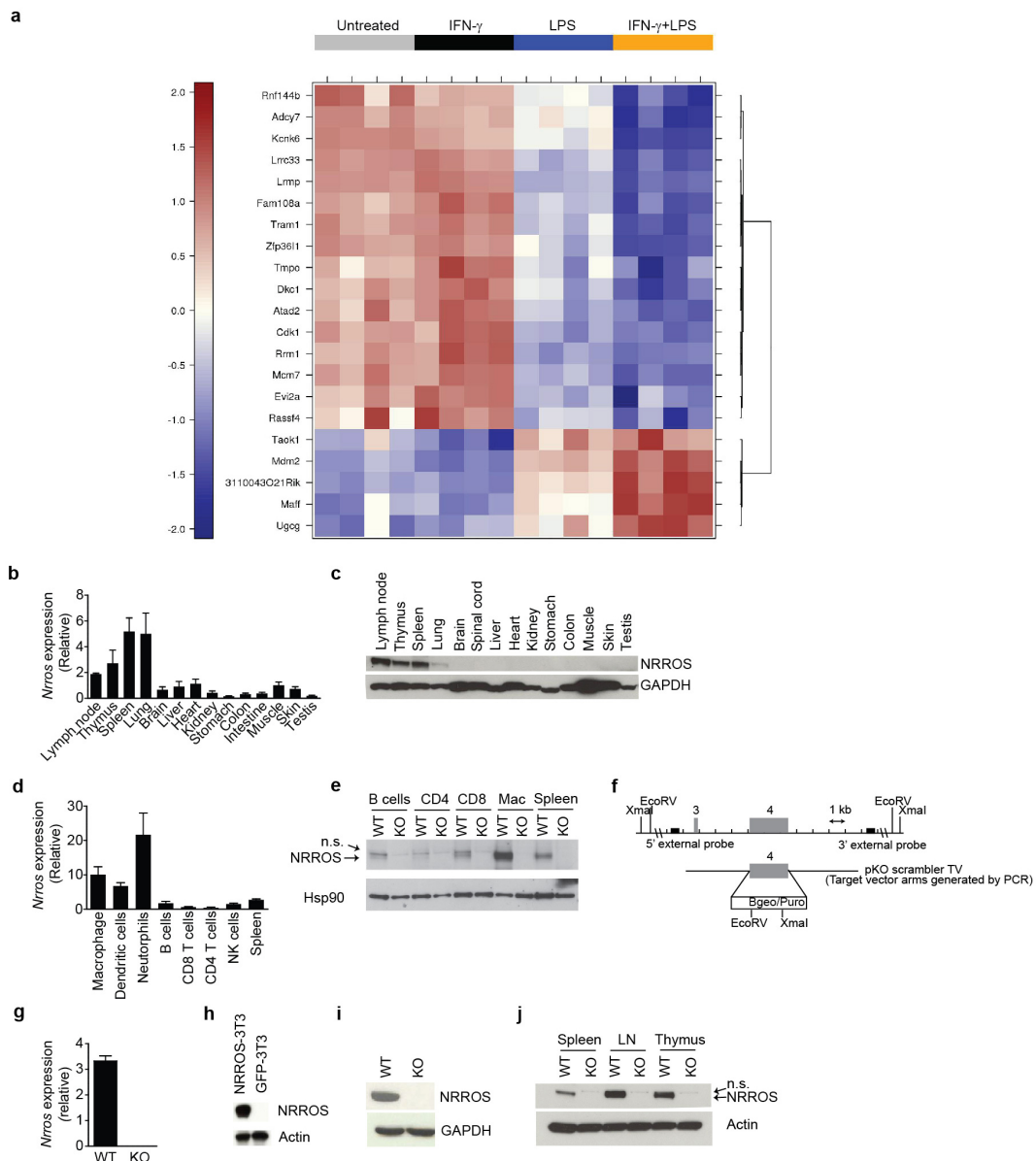
old and 8–12 weeks, or even longer, was allowed for reconstitution. Therefore, mice were 14–20 weeks old at the time of immunization. Male mice were used for most of the experiments. *Nrros*^{f/f} LysM-Cre^{pos} and *Nrros*^{f/f} LysM-Cre^{neg} mice used for data shown in Extended Data Fig. 5 were 6–8 weeks old.

A sample size of at least five mice per genotype was used in each independent experiment. No animals were excluded from any study. No blinding or randomization method was used in grouping the mice.

Measurement of oxidative damage in CNS tissues. Oxidative damage in the CNS of EAE-induced mice was assessed by measuring malondialdehyde levels⁴⁰. Brain and spinal cords from EAE-induced mice were collected and homogenized in PBS. Protein estimation was done by BCA assay. Homogenates were used to measure the levels of MDA by ELISA using OxiSelect MDA adduct ELISA kit (Cell Biolabs) or by western blot using OxiSelect MDA immunoblot kit (Cell Biolabs) according to the manufacturer's recommendations.

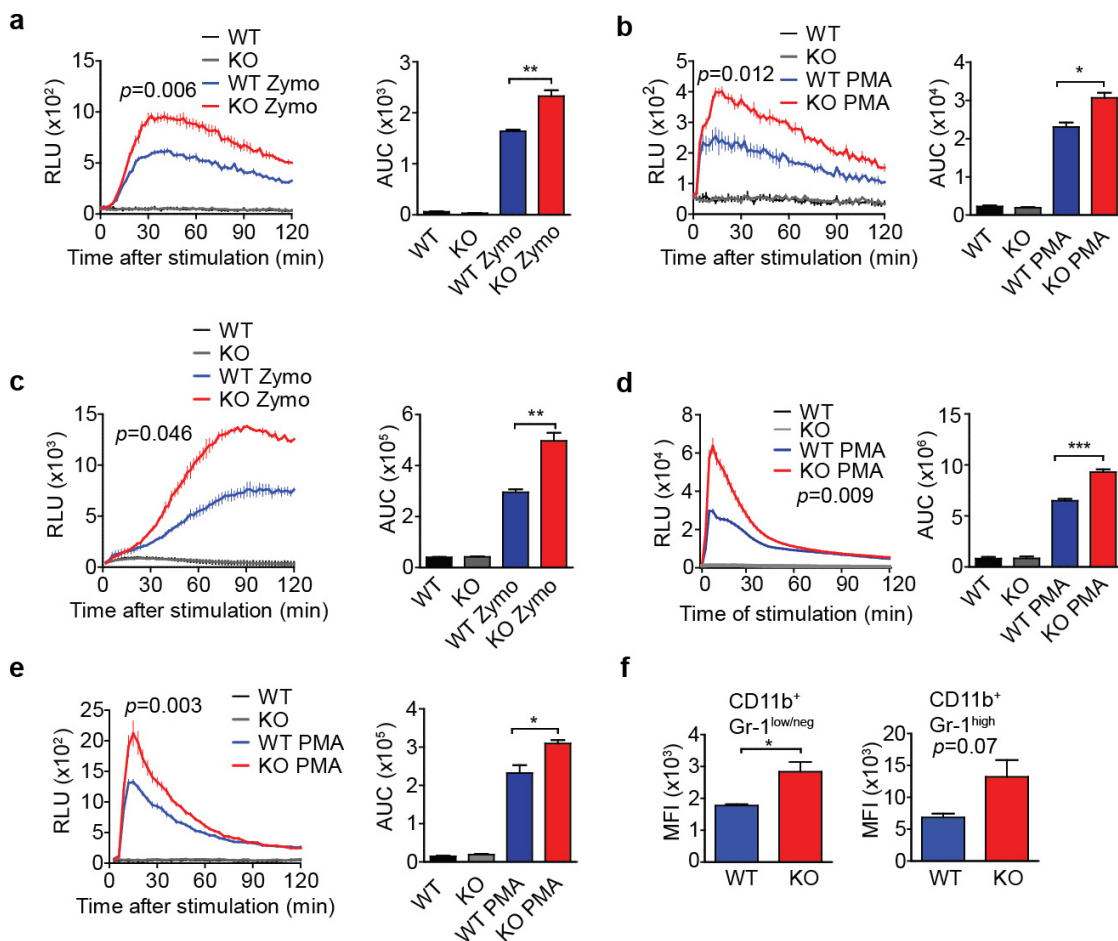
Statistical analysis. Statistical significance was calculated by Prism 5 software (Graphpad) using appropriate statistical test mentioned in the figure legends. For ROS measurements by luminol, area under curve (AUC) was calculated for each individually stimulated sample (at least three samples per group). The AUC values were then used in unpaired *t*-test with Welch's corrections to generate a *P* value for each experiment. The average AUCs from different experiments were used in paired *t*-test assuming equal variance to generate *P* values when comparing multiple experiments. Any other appropriate statistical methods applied for a data set are described in the figure legends. A *P* value of less than 0.05 was considered as significant.

25. Tang, T. *et al.* A mouse knockout library for secreted and transmembrane proteins. *Nature Biotechnol.* **28**, 749–755 (2010).
26. Mantel, A. *et al.* siRNA stabilization prolongs gene knockdown in primary T lymphocytes. *Eur. J. Immunol.* **38**, 2616–2625 (2008).
27. Irizarry, R. A. *et al.* Exploration, normalization, and summaries of high density oligonucleotide array probe level data. *Biostatistics* **4**, 249–264 (2003).
28. Bourgon, R., Gentleman, R. & Huber, W. Independent filtering increases detection power for high-throughput experiments. *Proc. Natl. Acad. Sci. USA* **107**, 9546–9551 (2010).
29. Smyth, G. K. Linear models and empirical bayes methods for assessing differential expression in microarray experiments. *Stat. Appl. Genet. Mol. Biol.* **3**, Article3 (2004).
30. Benjamini, Y. & Hochberg, Y. Controlling the false discovery rate: a practical and powerful approach to multiple testing. *J. Roy. Stat. Soc. B* **57**, 289–300 (1995).
31. Abbas, A. R. *et al.* Immune response in silico (IRIS): immune-specific genes identified from a compendium of microarray expression data. *Genes Immun.* **6**, 319–331 (2005).
32. Sayers, E. W. *et al.* Database resources of the National Center for Biotechnology Information. *Nucleic Acids Res.* **40**, D13–D25 (2012).
33. Li, Y. *et al.* Enrichment of endoplasmic reticulum with cholesterol inhibits sarcoplasmic-endoplasmic reticulum calcium ATPase-2b activity in parallel with increased order of membrane lipids: implications for depletion of endoplasmic reticulum calcium stores and apoptosis in cholesterol-loaded macrophages. *J. Biol. Chem.* **279**, 37030–37039 (2004).
34. DeLeo, F. R. *et al.* Processing and maturation of flavocytochrome b558 include incorporation of heme as a prerequisite for heterodimer assembly. *J. Biol. Chem.* **275**, 13986–13993 (2000).
35. Barry, K. C., Fontana, M. F., Portman, J. L., Dugan, A. S. & Vance, R. E. IL-1 α signaling initiates the inflammatory response to virulent *Legionella pneumophila* *in vivo*. *J. Immunol.* **190**, 6329–6339 (2013).
36. Green, S. A., Zimmer, K. P., Griffiths, G. & Mellman, I. Kinetics of intracellular transport and sorting of lysosomal membrane and plasma membrane proteins. *J. Cell Biol.* **105**, 1227–1240 (1987).
37. Czuprynski, C. J., Canono, B. P., Henson, P. M. & Campbell, P. A. Genetically determined resistance to listeriosis is associated with increased accumulation of inflammatory neutrophils and macrophages which have enhanced listericidal activity. *Immunology* **55**, 511–518 (1985).
38. Nikić, I. *et al.* A reversible form of axon damage in experimental autoimmune encephalomyelitis and multiple sclerosis. *Nature Med.* **17**, 495–499 (2011).
39. Hu, Y. *et al.* IL-17RC is required for IL-17A- and IL-17F-dependent signaling and the pathogenesis of experimental autoimmune encephalomyelitis. *J. Immunol.* **184**, 4307–4316 (2010).
40. Barabutis, N. & Schally, A. V. Antioxidant activity of growth hormone-releasing hormone antagonists in LNCaP human prostate cancer line. *Proc. Natl. Acad. Sci. USA* **105**, 20470–20475 (2008).



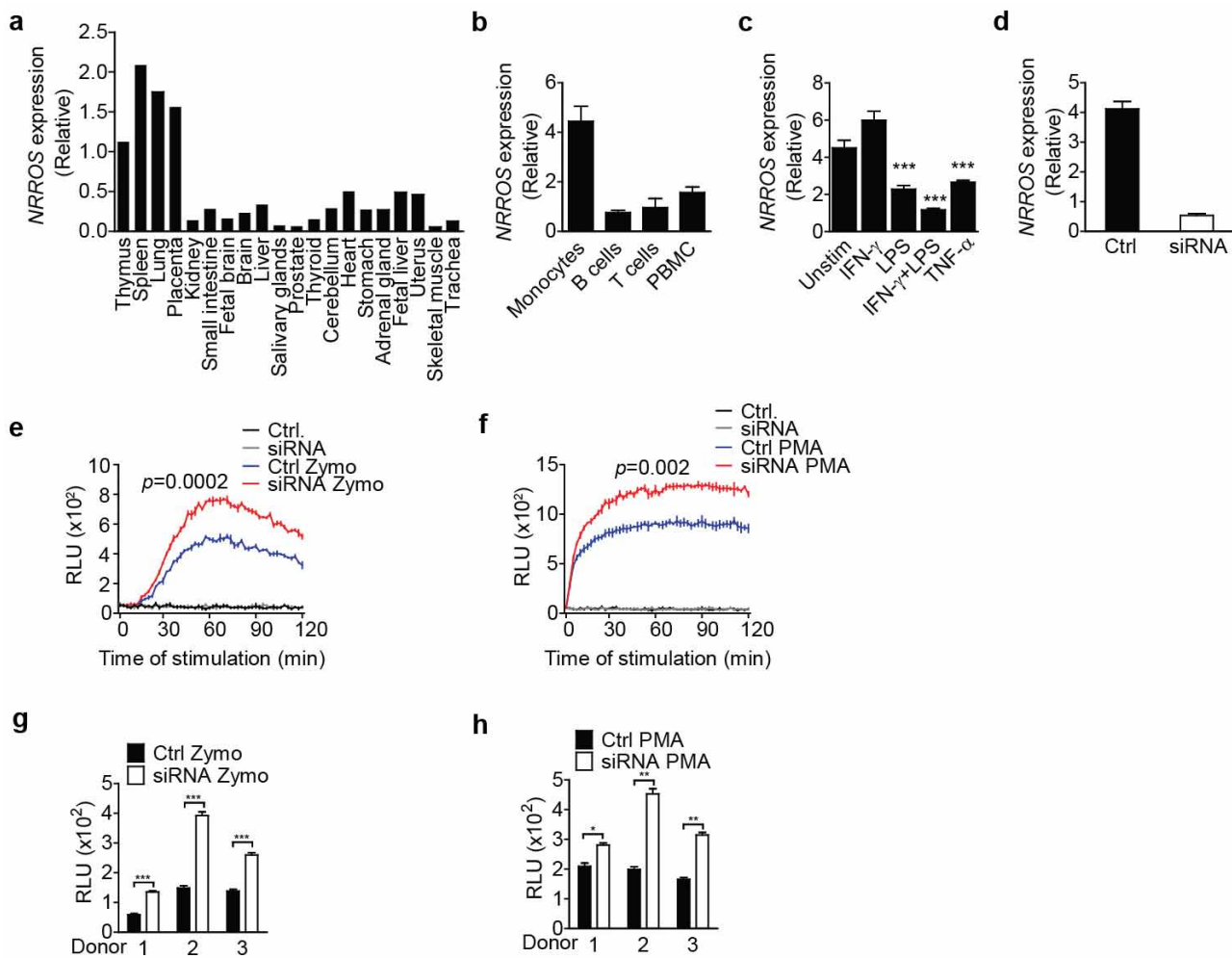
Extended Data Figure 1 | Murine NRROS is primarily expressed in immune tissues, especially in phagocytes. **a**, BMDMs were either untreated or treated with IFN- γ , LPS or both. Heat map displays genes that were preferentially expressed in leukocytes and differentially regulated by the synergistic effects of both the treatments compared to either treatment alone. **b**, Analysis of *Nrrros* expression in total RNA from different mouse tissues. Expression levels were normalized to *Rpl19* ($n = 4$). **c**, Western blot analysis of NRROS protein expression in different mouse tissues. GAPDH used as loading control. **d**, Analysis of *Nrros* expression in total RNA from immune cells sorted from mouse spleen, normalized to *Rpl19* ($n = 3–5$). **e**, Western blot analysis of NRROS protein expression in the indicated cells. HSP90 used as loading control. Mac, peritoneal macrophage; n.s., non-specific band observed only in lymphoid cells but not in macrophages with anti-NRROS antibody.

f, Schematic of the strategy used to generate NRROS-deficient mice. **g**, Analysis of *Nrros* expression in total RNA from spleens of WT and KO mice ($n = 5$), normalized to *Rpl19*. **h**, Western blot analysis of NRROS protein expression in 3T3 cells overexpressing NRROS (NRROS-3T3) and control cells (GFP-3T3) to screen anti-NRROS antibody. Actin used as loading control. **i**, Western blot analysis of NRROS protein expression in WT and KO BMDMs. GAPDH as loading control. **j**, Western blot analysis of NRROS protein expression in immune tissues from WT and KO mice. Actin used as loading control. Although there was no detectable specific band in KO BMDMs, a weak, nonspecific band was observed in lymphoid cells from both WT and KO mice that was present just above the specific NRROS band. Error bars, s.e.m. Data in **c**, **e** and **j** are representative of at least three independent experiments.



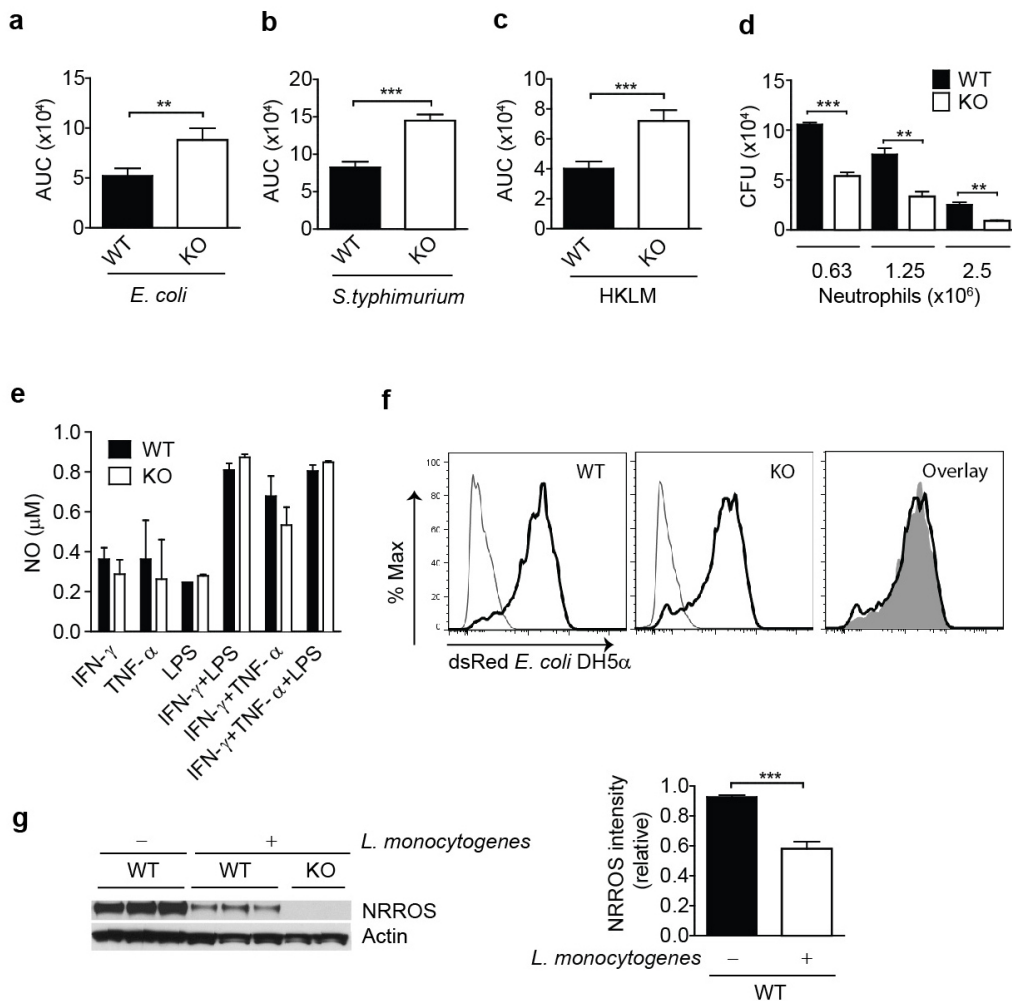
Extended Data Figure 2 | NRROS negatively regulates ROS production in various myeloid subsets. **a–e**, ROS production in thioglycollate-elicited peritoneal macrophages (**a, b**), neutrophils (**c, d**) and BMDM (**e**) stimulated with zymosan (zymo) (**a, c**) and phorbol 12-myristate 13-acetate (PMA) (**b, d, e**). Cells in **a, b, e** were primed with IFN- γ before ROS induction. Left panels, ROS kinetic plots of one representative experiment with three independent samples per group. Right panels, AUC from at least three

independent experiments. **f**, ROS production in splenocytes from WT and KO mice ($n = 3$) stimulated with PMA in the presence of CM-H2DCFDA and analysed by FACS. MFI of CD11b⁺ Gr-1^{low/neg} cells (left) and CD11b⁺ Gr-1^{high} (right) are shown. Error bars, s.e.m. * $P < 0.05$, ** $P < 0.01$, *** $P < 0.001$. Unpaired Student's *t*-test with Welch's corrections (**a–e**, left), paired Student's *t*-test (**a–e**, right), unpaired Student's *t*-test (**f**). Data in **f** are representative of two independent experiments.



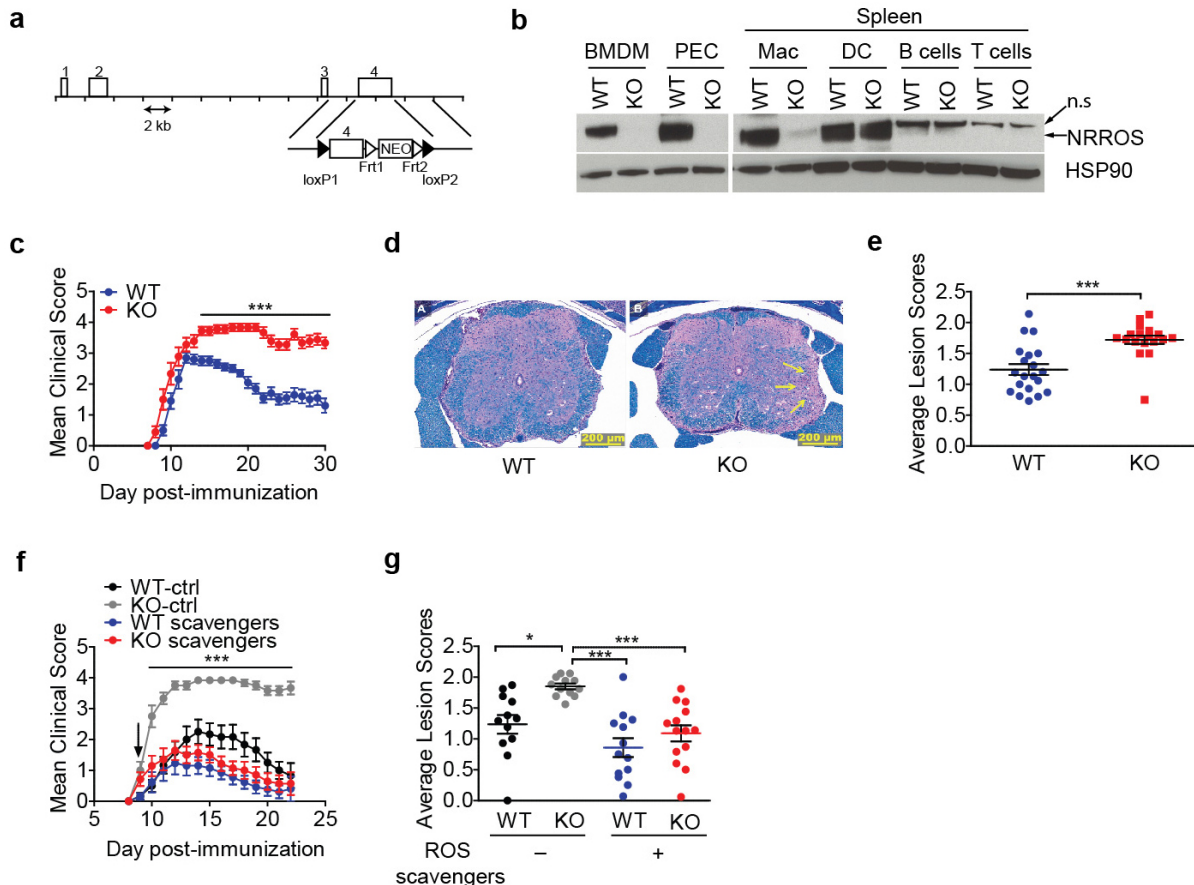
Extended Data Figure 3 | NRROS negatively regulates ROS production in human monocyte-derived macrophages (MDMs). **a, b**, Analysis of NRROS expression in total mRNA from human tissues (a) and cells purified from healthy donors (b) ($n = 3$). **c**, NRROS expression in MDMs stimulated as indicated ($n = 3$). **d**, NRROS expression in MDMs treated with non-targeting (Ctrl) or NRROS siRNA (siRNA). **e, f**, Kinetic graph of ROS production from cells shown in d. Cells were primed with IFN- γ and were then either

unstimulated or stimulated with zymosan (e) or PMA (f). **g, h**, ROS production by IFN- γ -primed MDMs stimulated, in triplicate, with zymosan (g) and PMA (h) from three individual donors. Values at the peak production (60 min) are shown. Data in a-d are normalized to endogenous control RPL19. Error bars, s.e.m. * $P < 0.05$, ** $P < 0.01$, *** $P < 0.001$. Unpaired Student's t-test with (e, f) and without (g, h) Welch's corrections. Data are representative of two independent experiments with three donors in each experiment.



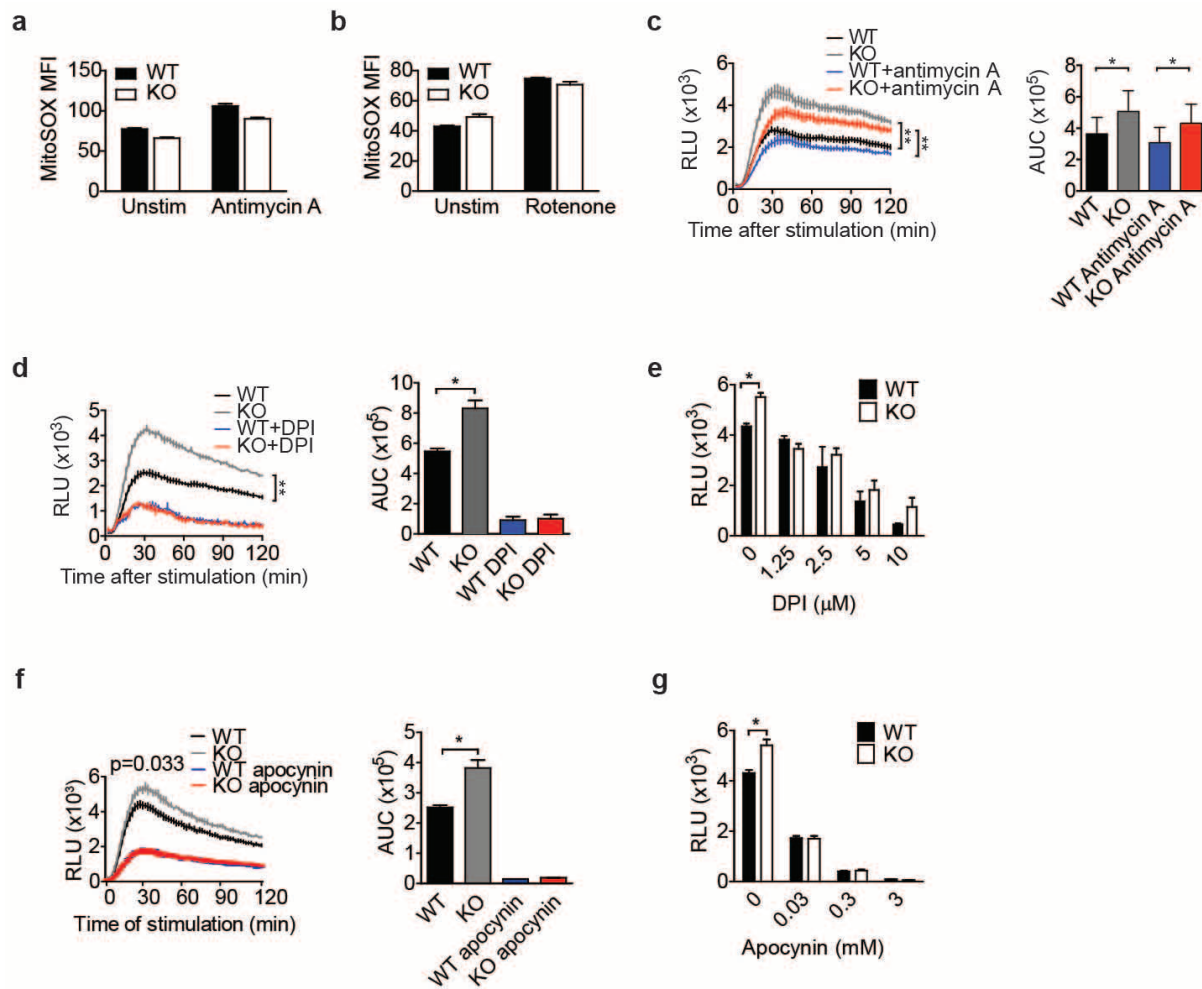
Extended Data Figure 4 | NRROS regulates ROS production and bactericidal activities of phagocytes but not phagocytosis or nitric oxide production by them. **a–c**, ROS production in IFN- γ -primed BMDMs stimulated with *E. coli* (a), *S. typhimurium* (b) and heat-killed *L. monocytogenes* (HKLM) (c). Averaged AUC from at least four independent experiments is plotted as bar graphs. **d**, *In vitro* *E. coli* killing by neutrophils purified from bone marrow of either WT or KO mice ($n = 3$). **e**, Nitric oxide (NO) in culture supernatant of BMDMs stimulated as indicated ($n = 3$). **f**, Representative

histograms showing phagocytosis of serum-opsonized dsRed-*E. coli* by BMDMs. Thin line, untreated cells; thick line, treated cells. In the overlay histograms on the right: filled area, WT cells; thick line, NRROS-deficient cells. **g**, Left, NRROS expression in CD11b $^{+}$ cells purified from spleens of uninfected WT and *L. monocytogenes*-infected WT and KO mice. Actin used as loading control. Right, densitometry analyses relative to actin. Error bars, s.e.m. ** $P < 0.01$, *** $P < 0.001$. Paired (a–c) or unpaired (d, g) Student's *t*-test. Data in d–g are representative of at least two independent experiments.



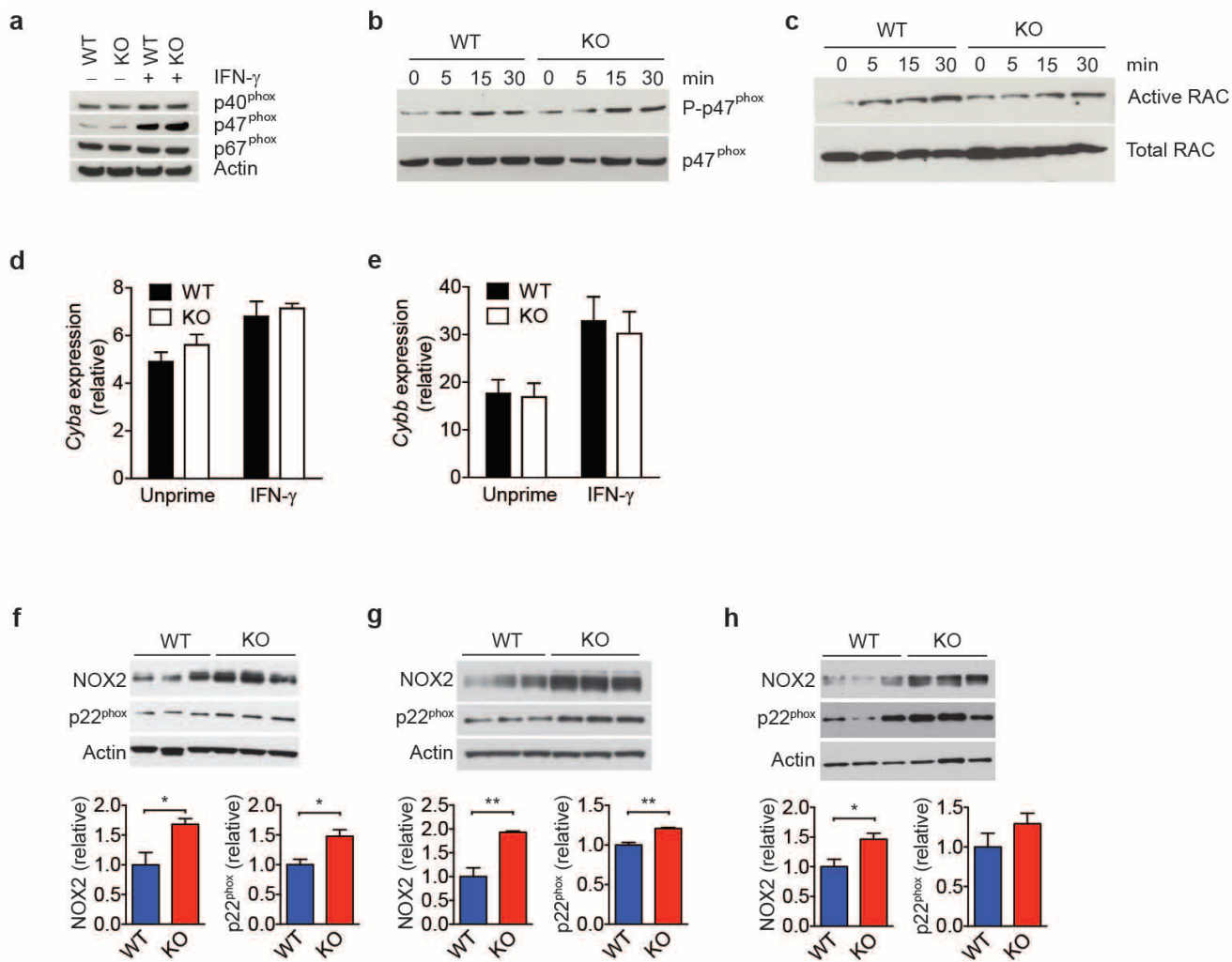
Extended Data Figure 5 | Myeloid-specific deletion of NRROS leads to exacerbated EAE. **a**, Schematic of the strategy used to generate *Nrros*^{fl/fl} mice. Numbers represent exons in *Nrros* gene. WT, *Nrros*^{fl/fl} LysM-Cre^{neg}; KO, *Nrros*^{fl/fl} LysM-Cre^{pos}. **b**, Western blot analysis of NRROS protein in immune cells from WT and KO mice. Actin used as loading control. Mac, macrophage; PEC, peritoneal macrophage. **c–e**, Clinical course (**c**), representative images of the spinal cord haematoxylin and eosin staining (**d**), and average histopathological lesion scores (day 30) (**e**) of EAE-induced WT ($n = 20$) and KO ($n = 18$) mice. Arrows in **d** indicate extensive myelinopathy of the lateral

white matter tracts. Luxol fast blue staining of myelin is in blue. **f, g**, Clinical course (**f**) and lesion severity as assessed by histopathology on day 30 (**g**) of EAE-induced WT and KO mice administered with either vehicle control (ctrl) ($n = 12$) or a cocktail of ROS scavengers ($n = 13$ for WT and $n = 14$ for KO) every 12 h starting from day 9 (arrow) for the rest of the study. Error bars, s.e.m. * $P < 0.05$, *** $P < 0.001$. Two-way (**c, f**) or one-way (**g**) analysis of variance followed by Bonferroni's post-hoc analysis, unpaired Student's *t*-test (**e**). Data are representative of at least three (**c–e**) and two (**b**) independent experiments. Data in **f, g** are combined from two independent experiments.



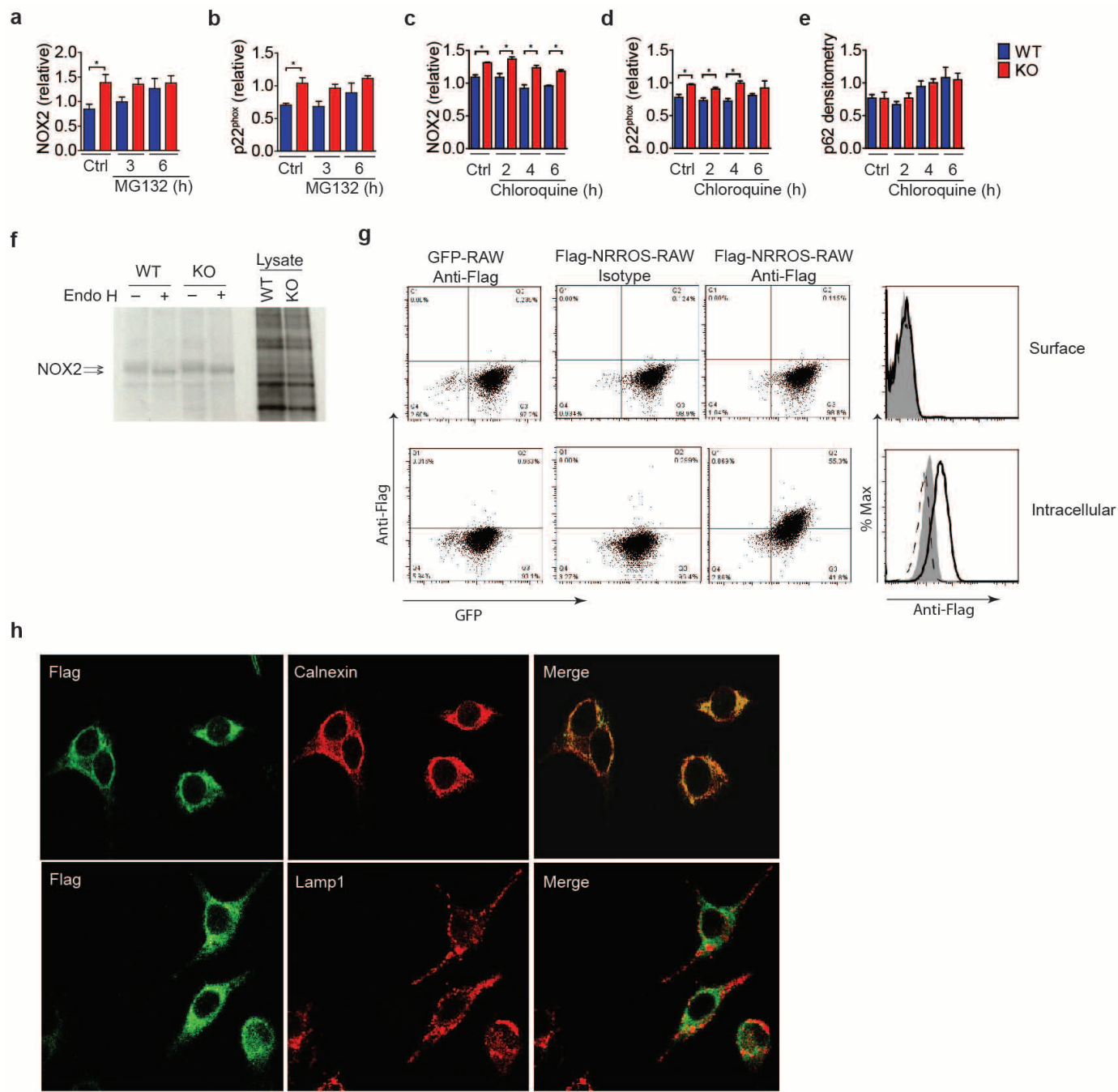
Extended Data Figure 6 | NRROS regulates NOX2-mediated ROS but not mROS generation. **a, b**, mROS production by IFN- γ -primed BMDMs from WT and NRROS-deficient (KO) mice stimulated with antimycin A (a) or rotenone (b) in the presence of MitoSOX. **c–g**, IFN- γ -primed BMDMs were pre-treated for 1 h with antimycin A (c), DPI (d, e) or apocynin (f, g) before ROS induction by zymosan. (c, d, f). Left panels, ROS kinetic plots of a representative experiment with three independent samples per group; right

panels, averaged AUC from three independent experiments. **e, g**, Dose response of DPI (e) or apocynin (g) treatment in WT and KO cells. Values at the peak of the curve are used for the bar graph. Error bars, s.e.m. * $P < 0.05$, ** $P < 0.01$. Unpaired Student's *t*-test with Welch's corrections (c, d, f, left), paired Student's *t*-test (c, d, f, right), unpaired Student's *t*-test (e, g). Data are representative of two (a, b, e, g) or three (c, d, f) independent experiments.



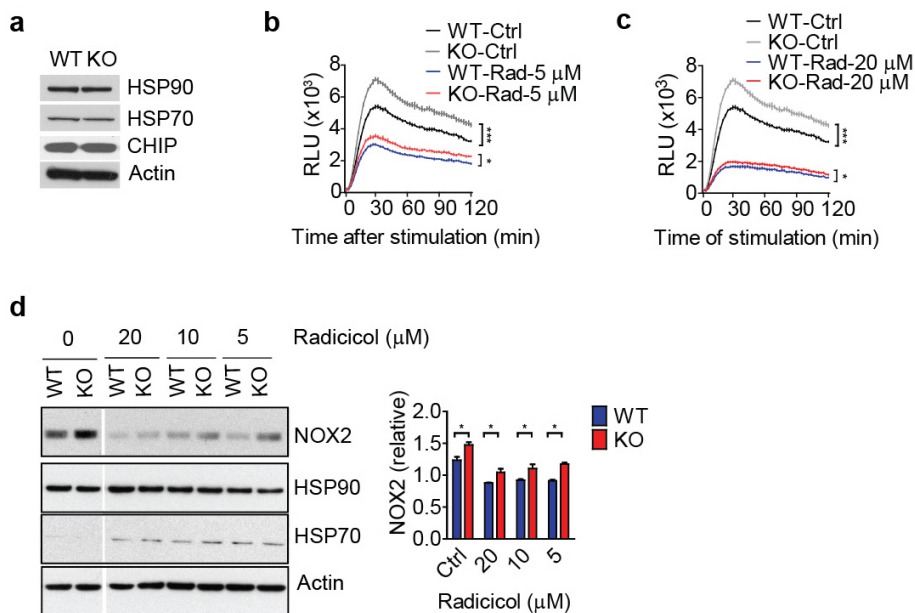
Extended Data Figure 7 | No difference between WT and NRROS-deficient BMDMs in expression and activation of the cytosolic members of NADPH oxidase complex. **a**, Western blot analysis of p40 $^{\text{phox}}$, p47 $^{\text{phox}}$ and p67 $^{\text{phox}}$ in the lysates of BMDMs from WT and NRROS-deficient (KO) mice either unprimed (–) or primed (+) with IFN- γ . Actin used as loading control. **b**, **c**, phospho-p47 $^{\text{phox}}$ (P-p47 $^{\text{phox}}$) and total p47 $^{\text{phox}}$ (**b**), active Rac and total Rac (**c**) in IFN- γ -primed BMDMs stimulated with zymosan for the indicated time. Active Rac was immunoprecipitated and blotted. Total Rac in the lysates used as control. **d**, **e**, Taqman analysis of Cyba (p22 $^{\text{phox}}$) (**d**) and Cybb (NOX2) (**e**) expression in total RNA from BMDMs either primed with IFN- γ or left alone (Unprime). Expression levels were normalized to endogenous control, ribosomal protein L19 (Rpl19) ($n = 3$). **f**–**h**, Top panels, NOX2 and p22 $^{\text{phox}}$ expression in thioglycollate-elicited peritoneal macrophages (**f**), in splenocytes from mice infected with *L. monocytogenes* for 24 h (**g**) and in total CNS cells from EAE-induced mice on day 15 post-immunization (**h**). Bottom panels, densitometry analyses relative to actin ($n = 3$). Error bars, s.e.m. * $P < 0.05$, ** $P < 0.01$ (unpaired Student's *t*-test). Data are representative of three (**a**–**c**) and two (**f**–**h**) independent experiments.

(e) expression in total RNA from BMDMs either primed with IFN- γ or left alone (Unprime). Expression levels were normalized to endogenous control, ribosomal protein L19 (Rpl19) ($n = 3$). **f**–**h**, Top panels, NOX2 and p22 $^{\text{phox}}$ expression in thioglycollate-elicited peritoneal macrophages (**f**), in splenocytes from mice infected with *L. monocytogenes* for 24 h (**g**) and in total CNS cells from EAE-induced mice on day 15 post-immunization (**h**). Bottom panels, densitometry analyses relative to actin ($n = 3$). Error bars, s.e.m. * $P < 0.05$, ** $P < 0.01$ (unpaired Student's *t*-test). Data are representative of three (**a**–**c**) and two (**f**–**h**) independent experiments.



Extended Data Figure 8 | NRROS is an ER protein and regulates proteasome-mediated degradation of NOX2 and p22^{phox} proteins.
a–e, Densitometry analyses relative to actin of NOX2 (**a**, **c**), p22^{phox} (**b**, **d**) and p62 (**e**) in IFN-γ-primed BMDMs from WT and KO cells treated with MG132 (**a**, **b**) or chloroquine (**c**–**e**) for the indicated period ($n = 3$). p62 is shown as positive control for chloroquine treatment. **f**, Autoradiography showing immunoprecipitated NOX2 from BMDMs metabolically labelled with [³⁵S]methionine for 1 h. The immunoprecipitates were subjected to Endo H treatment for 18 h. Total proteins in the flow-through lysates is shown as loading control. **g**, RAW cells retrovirally transduced to stably express GFP (GFP-Raw) or Flag–NRROS (Flag-NRROS-Raw) were stained with either isotype control (second column) or anti-Flag antibody (first and third

columns). Cells were either non-permeabilized (top panels) or permeabilized (bottom panels). Overlay of the three populations is shown on the right. Thick line, Flag-NRROS-Raw cells stained with anti-Flag; filled area, GFP-Raw cells stained with anti-Flag; dashed line, Flag-NRROS-Raw cells stained with isotype control. **h**, RAW cells stably expressing Flag-tagged NRROS were stained with anti-Flag antibody (Flag) (green) and one of the indicated organelle markers (red), calnexin (top row) and Lamp1 (bottom row) and imaged by confocal microscopy. Colocalization of the two colours is depicted by yellow colour in the merged images on the right column. Error bars, s.e.m. * $P < 0.05$ (unpaired Student's *t*-test). Data are representative of at least three independent experiments.



Extended Data Figure 9 | NRROS does not regulate NOX2 through the HSP90–HSP70–CHIP pathway. **a**, Western blot analysis of HSP90, HSP70 and CHIP in total lysates from IFN- γ -primed WT and KO BMDMs. Actin used as loading control. **b, c**, Zymosan-induced ROS production by IFN- γ -primed BMDMs treated with the HSP90 inhibitor radicicol at 5 μ M (b) and 20 μ M (c). A representative plot of kinetics of ROS production (three independently stimulated samples per group) from three independent experiments is shown.

d, Left, NOX2, HSP90 and HSP70 expression in IFN- γ -primed BMDMs treated with the indicated dose of radicicol. Actin used as loading control. Right, densitometry analyses relative to actin from three experiments. Error bars, s.e.m. * $P < 0.05$, *** $P < 0.001$. Unpaired Student's *t*-test with (b, c) and without (d) Welch's corrections. Data in **a** are representative of three experiments.

Extended Data Table 1 | Analysis of immune cell subsets in lymph node, spleen, thymus and blood of WT and KO mice

Lymph node	WT (n=5)	KO (n=5)
CD4 ⁺	64.1 ± 1.00	65.8 ± 0.62
CD8 ⁺	25.6 ± 0.67	24.5 ± 0.32
B220 ⁺	14.9 ± 0.86	15.6 ± 1.14
CD4 ⁺ CD25 ⁺	2.5 ± 0.10	2.7 ± 0.13

Spleen	WT (n=5)	KO (n=5)
CD4 ⁺	43.0 ± 0.98	45.1 ± 0.66
CD8 ⁺	24.0 ± 0.68	21.0 ± 0.86
B220 ⁺	42.9 ± 0.40	42.9 ± 1.85
γδ T cells	0.5 ± 0.05	0.5 ± 0.05
DX5 ⁺ (NK cells)	4.0 ± 0.25	4.02 ± 0.13
CD11b ⁺ F4/80 ⁺	4.1 ± 0.22	4.3 ± 0.07
CD11b ⁺ CD11c ⁺	0.5 ± 0.39	0.5 ± 0.03
CD11b ⁺ Gr-1 ⁺	3.2 ± 0.34	3.3 ± 0.11

Thymus	WT (n=5)	KO (n=5)
CD4 ⁺ CD8 ⁺	84.0 ± 1.14	84.3 ± 0.92
CD4 ⁻ CD8 ⁻	6.7 ± 0.78	7.1 ± 0.59
CD4 ⁺ CD8 ⁻	4.6 ± 0.43	4.2 ± 0.11
CD4 ⁻ CD8 ⁺	4.4 ± 0.38	4.8 ± 0.44

Complete Blood Count (CBC)	WT (n=5)	KO (n=5)
White blood cells	9.7 ± 1.67	10.0 ± 1.19
Neutrophils	9.7 ± 1.82	6.1 ± 0.95
Lymphocytes	81.3 ± 1.71	81.6 ± 2.87
Monocytes	6.5 ± 0.75	11.0 ± 3.02
Eosinophils	1.1 ± 0.29	0.6 ± 0.35
Basophils	1.4 ± 0.17	0.7 ± 0.44

Single-cell suspensions of lymph node, spleen and thymus were stained with the indicated surface marker and analysed by FACS. Percentages of cells in the total population are shown. Haematological analysis of the blood (complete blood count) showing the percentage of total white blood cells and the percentages of different leukocyte populations therein is shown. All the values are average ± s.e.m.